J. Physiol. (1986), **375**, *pp.* 195–227
With 13 *text-figures*
Printed in Great Britain

THE TRANSDUCTION CHANNEL OF HAIR CELLS FROM THE BULL-FROG CHARACTERIZED BY NOISE ANALYSIS

BY THOMAS HOLTON AND A. J. HUDSPETH

From the Physiological Laboratory, University of California School of Medicine S-762, San Francisco, CA 94143, U.S.A.

(*Received 21 June 1985*)

SUMMARY

1. Receptor currents in response to mechanical stimuli were recorded from hair cells in the excised epithelium of the bull-frog sacculus by the whole-cell, gigohm-seal voltage-clamp technique. The stimulus-dependent transduction current was separated from the cell's stimulus-independent K^+ and Ca^{2+} currents; the K^+ currents were blocked with an internal solution containing Cs^+ while the Ca^{2+} current was reduced by holding the membrane potential below -70 mV. The temperature of the preparation was maintained at about 10 °C to slow the kinetics of the cells' transduction channels.

2. Calibrated displacements of hair bundles of individual hair cells were made with a probe coupled by suction to the kinociliary bulb and moved with a piezoelectric-bimorph stimulator. The root mean square noise of probe motion was less than 2 nm. The mean, $\bar{I}$, and the variance, σ^2, of the receptor current were measured from the response to saturating ($\pm 0{\cdot}5$ μm) displacements of the hair bundle. $\bar{I}$ was corrected for current offsets and σ^2 for the transduction-independent background variance.

3. The relation between σ^2 and $\bar{I}$ is consistent with the predictions of a two-conductance-state model of the transduction channel, a model having only one non-zero conductance state. The relation between σ^2 and $\bar{I}$ was fitted by the equation $\sigma^2 = \bar{I}i - \bar{I}^2/N$, where N is the number of transduction channels in the cell and i is the current through a single open channel.

4. The conductance of the transduction channel is approximately ohmic with a reversal potential near 0 mV. The estimated conductance of a single transduction channel, γ, is $12{\cdot}7 \pm 2{\cdot}7$ pS (mean $\pm$ S.D.; $n = 18$) at 10 °C. γ is independent of the maximum transduction conductance of the cell, G_{max}.

5. The number of transduction channels, N, is proportional to G_{max}. N ranges from 7 to 280 in cells with G_{max} ranging from 0·08 to 2·48 nS. The largest values of N correspond to a few, perhaps four, active transduction channels per stereocilium.

6. Control experiments show that transduction by the hair cell of two artifactual sources of hair-bundle stimulation, noisy or discontinuous motion of the probe, do not contribute substantially to the measured variance, σ^2.

7. Displacement–response curves are generally sigmoidal and symmetrical; they reasonably fit the predictions of a two-kinetic-state model, comprising one open state and one closed state. The estimated displacement-sensitive free energy, Z, is $5{\cdot}7 \pm 1{\cdot}1$ kcal/mol μm (mean $\pm$ S.D., $n = 18$).

8. Power-spectral densities of the receptor current were measured in response to steps of displacement. On the assumption of the two-kinetic-state model, the data suggest that a bundle displacement that gives 30 % of maximum response corresponds to a mean lifetime of the channel in the open state of 0·9 ms at 9·5 °C or 130 μs at 37 °C.

INTRODUCTION

Hair cells, the sensory-receptor cells of the acousticolateralis system, transduce mechanical stimuli incident on their hair bundles into receptor potentials (for review, see Hudspeth, 1983). The key event in this mechanoelectric transduction process is the change in ionic conductance that occurs in a mechanically sensitive transmembrane pore, the 'transduction channel', as a result of applied force. Many of the basic properties of the transduction channel are unknown, or have been estimated only indirectly; for example, it is not known how many transduction channels occur in a cell, what the conductance of a single channel is, or precisely what the kinetic properties of the channel are.

In our experiments, which have been presented in preliminary form (Holton & Hudspeth, 1984, 1985), we have employed the whole-cell, gigohm-seal voltage-clamp technique (Marty & Neher, 1983) to measure currents from transduction channels in single hair cells of the saccular macula. Neither of the conventional physiological techniques used in previous experiments for recording receptor currents, the transepithelial voltage clamp (Corey & Hudspeth, 1983*a*, *b*) and the two-electrode voltage clamp (Corey & Hudspeth, 1979), has a band width wide enough or a background noise level low enough to resolve the currents from a small number of rapidly gated transduction channels in a single cell. Using the ensemble-variance method of data analysis (Neher & Stevens, 1977; Sigworth, 1980), we demonstrate that the receptor-current data reasonably fit the predictions of a two-conductance-state model of the transduction channel. On the assumption of this model, we estimate several fundamental biophysical properties of the transduction process, including the number of transduction channels in a single hair cell and the single-channel conductance. We also demonstrate that a description of the transduction channel comprising two kinetically distinguishable states adequately describes the receptor-current data. On the assumption of this model, we estimate basic kinetic properties of the channel: the displacement-sensitive free energy and the mean lifetime of the channel in the open state.

METHODS

Animal preparation

Experiments were performed on an epithelial preparation of hair cells from the saccular macula of the bull-frog (*Rana catesbeiana*) (Hudspeth & Corey, 1977). Each labyrinth was dissected from a pithed adult frog and maintained at 22 °C in an oxygenated external saline solution containing 110 mM-Na^+, 2 mM-K^+, 4 mM-Ca^{2+}, 118 mM-Cl^-, 3 mM = D-glucose and 5 mM-HEPES buffer with pH adjusted to 7·25. The saccular macula was dissected free and the otoconia removed. To aid in detaching the otolithic membrane that surmounts the hair bundles, the preparation was digested at 22 °C for 30–40 min in external saline to which was added 50 μg/ml subtilopeptidase BPN' (Sigma Chemical Company, St. Louis, MO, U.S.A.). The otolithic membrane was then removed with forceps and the preparation was transferred to the recording chamber, where it was held securely

with four fine tungsten clips. The chamber was mounted under a Zeiss WL microscope equipped with differential-interference-contrast optics. The preparation was continuously superfused with external saline at a rate of about 1 ml/min with a peristaltic pump (Minipuls 2, Gilson, Villiers-le-Bel, France). The superfusate was microfiltered (0·2 μm Acrodisc, Gelman, Ann Arbor, MI, U.S.A.) and chilled to less than 10 °C by a Peltier cooling device (Cambion 806-1000-01, Midland-Ross, Cambridge, MA, U.S.A.). Temperature was monitored to an accuracy of 0·1 °C (BAT-8, Bailey Instruments, Saddle Brook, NJ, U.S.A.) with a miniature thermocouple immersed in the chamber within 2 mm of the preparation. Temperature fluctuations in the chamber were observed to be less than $\pm$0·1 °C.

Recording procedures

Gigohm-seal electrodes were fabricated from 1·2 mm borosilicate glass (50 μl Microcaps, Drummond Scientific, Broomall, PA, U.S.A.) using standard techniques (Hamill, Marty, Neher, Sakmann & Sigworth, 1981). Each was pulled with a modified electrode puller (700D, David Kopf Instruments, Tujunga, CA, U.S.A.) and bent slightly to enable it to fit under the 40×, water-immersion objective lens so that the orifice of the pipette was nearly parallel to the cell's apical surface. The pipette was coated with silicone plastic (Sylgard 184, Dow Corning, Midland, MI, U.S.A.) to within 100 μm of the tip and heat polished to a tip diameter of 1–2 μm. In initial experiments electrodes were filled with our 'standard' internal solution, which contained 118 mM-Cs^+, 2 mM-K^+, 78 μM-Ca^{2+}, 2 mM-Mg^{2+}, 85 mM-aspartate, 4 mM-Cl^-, 1 mM-ATP, 1 mM-EGTA and 5 mM-HEPES buffer, buffered to pH 7·25. This solution provides a buffered Ca^{2+} concentration of 10 nM, Cs^+ to block the outward K^+ A-current and Ca^{2+}-activated K^+ current observed in these cells (Lewis & Hudspeth, 1983), and ATP and Mg^{2+} to maintain cellular metabolism. The bath ground electrode was an agar-filled glass pipette which contacted an AgCl-plated silver wire.

Forming gigohm seals between recording electrodes and the apical surfaces of hair cells proved much more difficult than forming seals on the basolateral surfaces of isolated cells (Lewis & Hudspeth, 1983). Seals occasionally formed with pipettes containing the standard internal solution described above, but these seals were generally evanescent and broke down when suction was applied to establish the whole-cell recording condition. We investigated the possibility that polycationic substances added to the internal solution would facilitate the formation of gigohm seals on the apical cellular surfaces, possibly by bridging the negatively charged groups on the surfaces of the glass and the membrane. Because aminoglycoside antibiotics are known to interact with the apical surfaces of hair cells, and indeed to cause the stereocilia within their hair bundles to fuse (Wersäll, Bjorkroth, Flock & Lundquist, 1973), we tried these compounds. The distal tips of pipettes were filled with approximately 1 μl of standard internal solution to which had been added 1 mM-gentamicin or dihydrostreptomycin sulphate (Sigma Chemical Company, St. Louis, MO, U.S.A.); the pipette was then backfilled with standard internal solution. Stable, high-impedance seals on hair cells could be made routinely using these pipettes. Pipettes were advanced towards the preparation under pressure (see below), so that effectively all of the drug in the tip was expelled from the pipette before it contacted the cell, a conclusion confirmed by observing pipettes with dye-filled tips. This suggests that the enhanced ability of aminoglycoside-treated pipettes to seal onto cells results, not from a bulk effect of the drug on the cell, but from molecules that adhere to the glass after the bulk of the drug has been ejected. Both gentamicin and streptomycin are known ototoxins which reversibly block transduction when applied iontophoretically to the apical surfaces of hair cells (Hudspeth & Kroese, 1983). But since the experimental chamber was continuously perfused with standard saline solution throughout recordings, it is unlikely that the transduction channels were permanently blocked by drugs expelled from the pipette prior to the formation of the gigohm seal. We were concerned about possible intracellular effects of any drugs remaining in the pipette. We found, however, that the amplitude and sensitivity of receptor currents recorded with pipettes treated with aminoglycosides were comparable to those measured in preliminary experiments using standard internal solution only. In addition, some recordings were made with pipettes whose tips were treated with 500 μM each of spermine and spermidine (Sigma Chemical Company, St. Louis, MO, U.S.A.) in the internal solution. These polyamines are normally present in nervous tissue at comparable concentrations (Seiler & Schmidt-Glenewinkel, 1975). Recordings made with these pipettes were also comparable to those made with untreated pipettes and with those treated with aminoglycosides.

The configuration of the recording electrode and the stimulus probe is shown in Fig. 1. Recording electrodes were attached to the headstage of the clamp (Mark V, Yale University Physiology Shop, New Haven, CT, U.S.A.) and advanced towards the epitheliuim with a Huxley-type micromanipulator (Frederick Haer, Brunswick, ME, U.S.A.). Slight positive pressure was applied to the electrode during its approach towards the cell to prevent contaminants at the air–fluid interface or in the bath from coating the tip of the electrode. When the electrode contacted the apical surface of the cell near the hair bundle, slight suction was transiently applied to form a gigohm seal. The stray capacitance of the electrode was then electrically neutralized, and further suction (5 kPa) was applied to rupture the membrane patch under the electrode, thereby establishing electrical and fluid

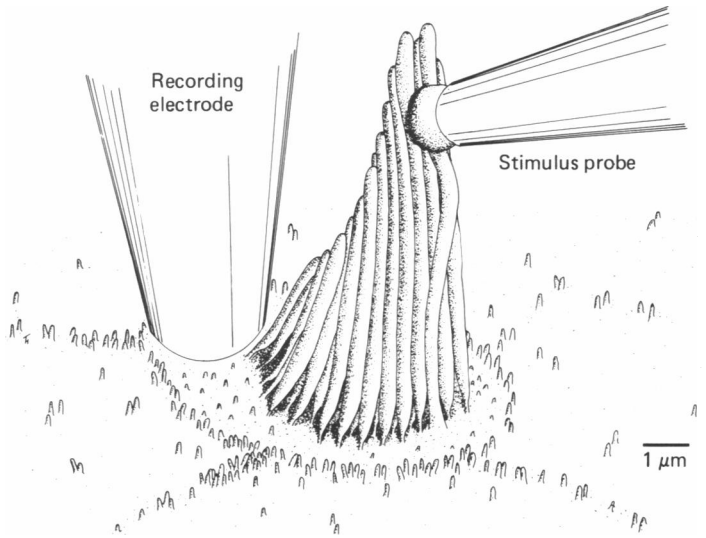

Fig. 1. A schematic diagram of the apical surface of one saccular hair cell with a recording electrode and stimulus probe in place. The recording electrode contacts the cell near the hair bundle, where it forms a gigohm seal. Calibrated displacements of the hair bundle are made with the glass stimulus probe moved by a piezoelectric-bimorph element. The stimulus probe is coupled by slight, constant suction to the kinociliary bulb of the hair bundle, which is approximately 7 μm above the surface of the cell. Positive displacement of the hair bundle, defined as motion towards the kinocilium, elicits an inward receptor current.

continuity with the cell, that is, the whole-cell recording configuration. A constant suction of 2 kPa was maintained in order to prevent a resealing of the membrane patch. Electrodes usually had series resistances during recordings of 4–10 MΩ, much of which was compensated by the voltage-clamp circuit. Control experiments confirmed that hair cells are not electrically or dye coupled to one another or to supporting cells; therefore, the currents that are measured from a single cell using the whole-cell voltage-clamp technique originate in that cell.

After establishing the whole-cell recording condition, we generally set the command voltage of the clamp to −60 mV. This holding potential was sufficiently negative to deactivate the hair cell's Ca^{2+} conductance (Lewis & Hudspeth, 1983; R.S. Lewis & A.J. Hudspeth, unpublished observations), yet not so negative as to activate the cell's inwardly rectifying conductance (Corey & Hudspeth, 1979). The actual membrane potential, V_m, was taken to be the command voltage plus the electrode-tip diffusion potential, which was measured using a KCl-filled agar bridge to be −13 mV. Except for the data of Fig. 4, we have not attempted to compensate V_m for the Donnan-equilibrium potential between the electrode and the cell due to the large, slowly diffusing anions in the cytoplasm (Fenwick, Marty & Neher, 1982; Marty & Neher, 1983). For most cells, the value of this potential is not known, although a slow shift in the voltage dependence of

inactivation of the hair cell's K^+ A-current (R. S. Lewis & A. J. Hudspeth, unpublished observations) suggests a value of up to −15 mV. Had we corrected V_m for a Donnan-equilibrium potential of −15 mV, our estimates of the single-channel conductance would have been about 20% higher.

The band width of the voltage-clamp amplifier, determined to first order by the uncompensated series (access) resistance of the electrode and the cell's membrane capacitance (Sigworth, 1983), was estimated in several cells from the rise time of the response to command-voltage steps of 10 mV to be at least 3 kHz. The noise floor of measurement is determined primarily by the series resistance of the electrode and the cell's impedance (Marty & Neher, 1983). Because of the appreciable membrane capacitance of the hair cell (about 15 pF), the noise floor rises near 1 kHz and limits our ability to resolve high-frequency, low-amplitude components in the power-spectral density of receptor-current noise.

Stimulation procedures

Stimulus probes were pulled and heat polished using procedures similar to those for making recording electrodes, but were not coated with Sylgard. Probes were filled with external saline, attached to a micromanipulator and advanced to contact the bulbous tip of the hair bundle's kinocilium (Fig. 1), which lies approximately 7 μm above the apical surface of the cell. Slight constant suction (2 kPa) was applied and maintained on the probe to keep it tightly coupled to the hair bundle. Calibrated displacements of the bundle, generally sinusoidal and 0·5 μm in peak amplitude, were made by moving the probe with an electrically shielded piezoelectric-bimorph stimulator (Corey & Hudspeth, 1980). The axis of motion of the stimulator was adjusted to be parallel to the epithelium's apical surface and to coincide with the hair bundle's plane of symmetry; the hair cell is maximally sensitive to stimulation along this axis (Shotwell, Jacobs & Hudspeth, 1981). A positive mechanical stimulus is defined as one that displaces the hair bundle towards the kinocilium, producing an inward receptor current. The peak displacement amplitude of 0·5 μm was chosen to saturate the receptor current at its maximum inward value for positive displacements and at zero for negative displacements.

Vibration isolation

To prevent unintentional mechanical stimuli such as vibration from the building and mechanical equipment from being coupled through the stimulus probe to the hair cells, the microscope, manipulators and associated components were magnetically fixed to the steel top of an air table (Serva-Bench IV, Barry Controls, Watertown, MA, U.S.A.). The micromanipulators used to position the stimulus and recording probes were also modified to increase their stability and were mechanically damped by the attachment of packets of lead shot.

Mechanical noise of the stimulus probe, defined as probe motion in the absence of intentional mechanical stimuli, was measured with a calibrated photodiode system (Corey & Hudspeth, 1980). The power-spectral density of probe noise (Fig. 2) reaches a maximum value of about 10^{-20} m^2/Hz at the lowest frequency measured (40 Hz) and falls below the noise floor of measurement (imposed by the illuminance level and the characteristics of the photodiode) for frequencies above 150 Hz. The root mean square (r.m.s.) value of the noise is 2 nm in the frequency range 40 Hz–1 kHz; since most of the spectral components of the noise are below the measurement noise floor, this value is an over-estimate of the probe's true noise.

Data acquisition

Measurement of the receptor current. Receptor currents were obtained in response to continuous sinusoidal stimuli produced by an oscillator (4100A, Krohn-Hite, Avon, MA, U.S.A.). The frequency of stimulation ranged from 20 to 40 Hz, with the exact frequency chosen to synchronize the stimulus with the computer's acquisition of response data; one period of the stimulus corresponded to an integral multiple of the interpoint time of the computer's analog-to-digital (A/D) converter, which ranged from 50 to 100 μs. A minimum of 128 samples was obtained per period of the stimulus; each data record comprised up to 4096 points, generally fourteen to sixteen cycles of response. Five to fifty data records were collected sequentially in each recording epoch and stored on disk for later analysis. Acquisition of each data record was synchronized to start at a zero crossing of the stimulus. Synchronization of the oscillator and computer remained within 10 μs at the end of the data record. In some experiments, gated sinusoidal stimuli with durations of 205–410 ms were generated by the computer synchronously with data sampling. The stimuli

consisted of five to ten cycles of a sinusoid, digitized at 256 points per cycle, with rising and falling portions shaped by a Gaussian envelope.

Aliasing of sampled data was limited by filtering the analog signal with an eight-pole active Butterworth filter (901F, Frequency Devices, Haverhill, MA, U.S.A.) with a cut-off frequency equal to half the sampling frequency. The output of the voltage-clamp amplifier, a voltage proportional to membrane current, was amplified and an offset was subtracted so that the peak-to-peak response of the cell filled a substantial fraction of the dynamic range of the 12-bit A/D converter. The quantization error expected to result from digitization of a 100 pA response is less than 0·05 pA.

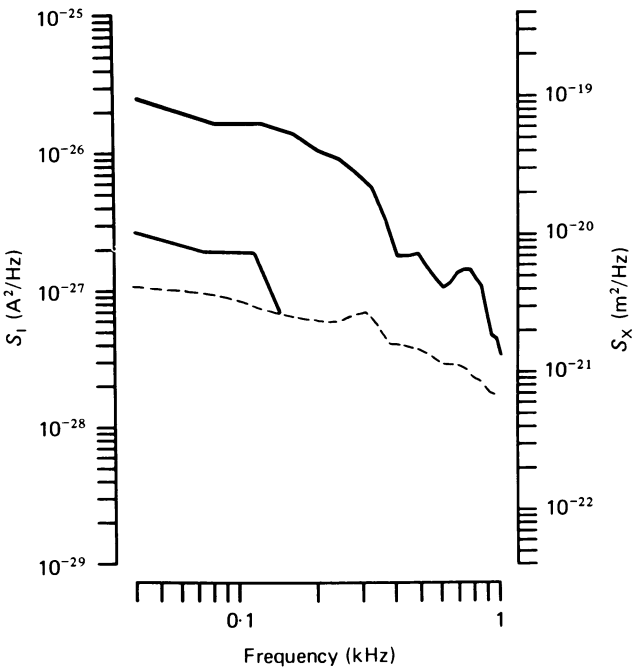

Fig. 2. $S_x(f)$ (lower continuous trace) is the power-spectral density of the motion of the tip of the stimulus probe in the absence of an intentional stimulus. The noise floor of the measurement (dashed line) is determined with the probe tip removed from the field of the photodiode. $S_I(f)$ (upper continuous trace) is the power-spectral density of the receptor current in response to a static displacement of the hair bundle that evokes a mean receptor current of 0·3 $\bar{I}_{max}$. $S_I(f)$ is obtained by subtracting from the spectrum of membrane current the background-noise spectrum, which is taken to be the spectrum of membrane current measured in response to a large, saturating displacement of the hair bundle. The ordinate scales are aligned to show the relation between $S_x(f)$ and $S_I(f)$ that would exist if the receptor-current noise were to result solely from transduction of probe motion by a cell whose peak slope sensitivity was 500 pA/μm.

Construction of displacement–response curves. Displacement–response curves were constructed by plotting the instantaneous magnitude of the receptor current against the position of the hair bundle. We did not measure the motion of the hair bundle; we assumed that the bundle was coupled tightly to the probe so that the bundle's position, $x(t)$, followed the driving voltage of the stimulus probe, $x(t) = A \cos(2\pi ft + \phi)$, where A is the peak amplitude of the probe's motion, f is the stimulus frequency and ϕ is the phase of the probe's motion with respect to the driving signal. A and ϕ, measured using a photodiode on one stimulus probe in a control experiment, were determined to good approximation by the filtering characteristics of the bimorph-stimulator electronics. A was adjusted to be 0·5 μm at 5 Hz, and decreased less than 5 % over the frequency range 5–40 Hz. When the stimulus wave form was corrected for ϕ at a given frequency, the resulting displacement–response

curve showed little hysteresis, that is, the response evoked by the positive- and negative-going phase of the probe's motion were almost superimposable. We took this as evidence that the probe was well coupled to the stimulus probe, and therefore that the receptor current was an instantaneous function of the probe's position; that is, there was no memory of the probe's previous position. We did not calibrate A and ϕ for each stimulus probe, but adjusted the phase correction of the stimulus wave form to minimize the observed hysteresis of the displacement–response curve. The value of ϕ obtained by this method rarely differed from the value measured in the control experiment by more than 0·02 rad. When the hysteresis had been minimized, the difference between the responses to positive- and negative-going phases of the stimulus did not exceed 8% of the maximum receptor-current amplitude at any position of the hair bundle.

Computation of power-spectral density. Power-spectral densities of receptor-current noise were computed from records of receptor current measured in response to step stimuli generated by the computer. Each stimulus consisted of a staircase displacement from the rest position (defined as 0 μm) to either the maximum positive displacement (+0·5 μm) or the maximum negative displacement (−0·5 μm) in one to three equal steps, followed by a return to 0 μm. The transition between steps was smoothed by a Gaussian envelope with a rise time (10–90% of maximum amplitude) of 8·1 ms. For each step, an integral multiple of 256 points of the receptor current was digitized at an interpoint time of 100 μs. Power-spectral densities were then computed from the steady-state portion of the data at each step. The duration of each staircase stimulus was 380–410 ms and the time between successive stimuli was at least 300 ms.

Data analysis

Computation of the receptor-current mean and variance. The total measured membrane current, I_m, is assumed to consist of two statistically independent components,

$$I_m = I + n. \tag{1}$$

I is the 'transduction-dependent' (receptor) current which arises from stochastic gating of the hair cell's transduction channels, modulated by stimulation of the cell's hair bundle. The mean of I with respect to time is denoted $\bar{I}$ and its variance is σ^2. n is the 'transduction-independent' background noise. The mean of n, denoted I_0, is termed the mean offset current; it derives primarily from d.c. instrumentation offsets and from the cell's leakage current. The variance of n, denoted σ_0^2, is termed the background variance. The principal source of background variance in whole-cell recording (Marty & Neher, 1983) arises from the access resistance of the recording pipette (4–10 MΩ) in series with the membrane capacitance of the cell (about 15 pF). From theoretical calculations or from noise measurements of the electrical equivalent network, the magnitude of this component of σ_0^2 can be determined to be at least 5·6 pA^2 over the frequency range 40 Hz–1 kHz. Other sources of background variance exist, but are probably substantially less important than the preceding one. For example, given a hair-cell input impedence in excess of 200 MΩ (Corey & Hudspeth, 1979), we calculate that the total thermal noise due to current across the cell's membrane is less than 0·5 pA^2; given a maximum hair-cell transduction conductance of about 2·5 nS (see below), the thermal noise of ions flowing through open transduction channels alone is not likely to exceed 0·2 pA^2. Another possible source of background variance, whose magnitude we have not estimated, arises from current flowing through unblocked K^+ and Ca^{2+} conductances. From eqn. (1), the mean ($\bar{I}_m$) and variance (σ_m^2) of the membrane current are given by

$$\bar{I}_m = \bar{I} + \bar{I}_0, \tag{2}$$

$$\sigma_m^2 = \sigma^2 + \sigma_0^2. \tag{3}$$

By measuring $\bar{I}_m$ and σ_m^2 from a cell and estimating $\bar{I}_0$ and σ_0^2, $\bar{I}$ and σ^2 can be obtained from eqns. (2) and (3).

$\bar{I}_m$ and σ_m^2 were measured from records of membrane current by the method of Sigworth (1980). For each data record, a local mean was computed by averaging all fourteen to sixteen response cycles in the record. The local variance was then computed by averaging the mean square difference between the local mean and each response cycle. The reason for computing local means and variances was to minimize the effect of drifts in current that could occur in recordings over the course of minutes. Grand averages of the membrane-current mean ($\bar{I}_m$) and variance (σ_m^2) were formed by averaging the local means and variances over all records. Records were excluded from

the computation of the grand averages of $\bar{I}_m$ and σ_m^2 if transient noise or discontinuities produced an unusually high local variance. Records were also excluded if the response amplitude changed markedly during the recording epoch, namely if the peak amplitude of the record's local mean differed by more than 10% from the peak amplitude of the local mean measured from the first record of the series.

The computation of $\bar{I}_0$ and σ_0^2 is based on the assumption that the mean ($\bar{I}$) and variance (σ^2) of the receptor current approach zero for large, negative hair-bundle displacements. For a channel described by the two-conductance-state model (see Appendix), this assumption is equivalent to assuming that $p(x)$, the probability of a channel's being open, is effectively zero for large, negative displacements. Given measurements of the minimum ($(\sigma_m^2)_{min}$) and maximum ($(\sigma_m^2)_{max}$) values of the membrane-current variance and an estimate of the background variance (σ_0^2), it can be shown that the minimum probability of the channel's being open, p_{min}, has an upper bound

$$p_{min} \sim \frac{1}{4} \frac{(\sigma_m^2)_{min} - \sigma_0^2}{(\sigma_m^2)_{max} - \sigma_0^2}. \quad (4)$$

Substituting typical values of $(\sigma_m^2)_{max} = 55$ pA^2, $(\sigma_m^2)_{min} = 8$ pA^2 and $\sigma_0^2 \geqslant 6$ pA^2 (Fig. 5*D*) into eqn. (4) gives a lower bound of $p_{min} \leqslant 0{\cdot}01$. This result supports the assumption that all the transduction channels are effectively closed for large, negative hair-bundle displacements, so that the mean and variance of the receptor current approach zero. From eqns. (2) and (3), this implies that $\bar{I}_0$ and σ_0^2 are respectively the mean and variance of the membrane current measured at these large, negative displacements. Records were chosen for analysis only if the membrane current saturated at its minimum value for the largest negative displacements. For these records, we calculated $\bar{I}_0$ by determining the range of displacements over which $\bar{I}_m$ was within 2% of the minimum value; $\bar{I}_0$ was the average of $\bar{I}_m$ over this displacement range. σ_0^2 was either the minimum or the average value of σ_m^2 over the same range.

Ensemble-variance analysis. The ensemble-variance method of analysis (Sigworth, 1980) involves measuring $\bar{I}$ and σ^2 and then, on the assumption that the two-conductance-state model of the transduction channel applies (see Appendix), fitting a parabola to plots of σ^2 against $\bar{I}$ (mean–variance plots) according to eqn. (9) to derive values for N, the number of transduction channels in a cell and i, the single-channel current. The ensemble-variance method does not require stationarity of the membrane current and is therefore appropriate for studying displacement-modulated conductances such as the transduction conductance of the hair cell. As discussed above, we have estimated the mean and variance of the receptor current (eqns. (2) and (3)) on the assumption that $p_{min} = 0$. If $p_{min} > 0$, it can be shown that the estimated value of i is lower than the true value by at most a factor of $(1-2\,p_{min})$ while the estimated value of N does not differ from the true value. Given a value of $p_{min} \leqslant 0{\cdot}01$, our estimate of i differs from the true value by less than 2%.

RESULTS

The following sections detail properties of the receptor current recorded with gigohm-seal electrodes from thirty-three hair cells in over fifty saccular maculae. The first section demonstrates that the relation between the mean and variance of the receptor current agrees with the predictions of the two-conductance-state model of the transduction channel described in the Appendix. The ensemble-variance technique is used to arrive at estimates for the number of transduction channels in a single cell and for the conductance of a single channel. The second section demonstrates that receptor-current data, such as displacement–response curves, are reasonably fitted by a particular two-conductance-state model of the channel, the two-kinetic-state model. The mean open time of the channel on the assumption of this model is estimated from the power-spectral density of receptor-current noise.

The two-conductance-state model of the transduction channel

Measurement of the hair-cell receptor current. Fig. 3 shows four cycles of the receptor current evoked by displacing the hair bundle of a hair cell with a 25 Hz sinusoidal stimulus. In most cells, a 1 μm peak-to-peak sinusoidal stimulus was sufficient to drive the receptor current essentially into saturation, evoking a maximum inward current, $\bar{I}_{max}$, for positive displacements, and zero response for negative displacements. The maximum response amplitude obtained in this study was -221 pA, and most amplitudes were between -50 and -150 pA. The maximum response sensitivities

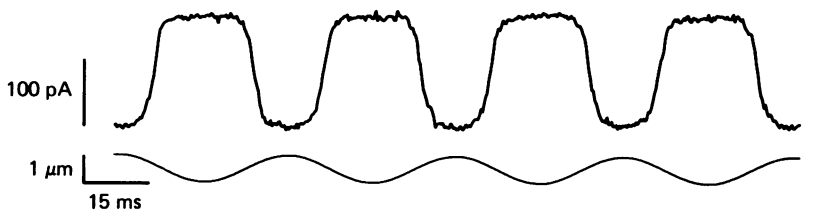

Fig. 3. Four cycles of the receptor current (upper trace) evoked by displacing the hair bundle with a 25 Hz sinusoidal stimulus (lower trace). Inward (negative) receptor current is plotted downward. The stimulus trace is the electrical signal to the probe, with phase adjusted to minimize the hysteresis of the response as described in the text. A $\pm 0{\cdot}5$ μm probe displacement at the level of the kinociliary ball corresponds, on average, to a ± 71 mrad angular displacement of the stereocilia.

exceeded 500 pA/μm. These response amplitudes and sensitivities are comparable to those measured in hair cells voltage clamped with two conventional micro-electrodes (Corey & Hudspeth, 1979). Thus it appears that the whole-cell recording method does not grossly compromise the cells' response properties. Response amplitudes were generally greatest at the moment of initial recording and often remained stable for several minutes thereafter, drifting less than 5% over the recording period. Except where noted, the results presented here are derived from stable recording intervals.

Current–voltage relation. In two cells we measured current–voltage relations of receptor current in response to gated sinusoidal stimulation of the hair bundle. For the cell whose data are shown in Fig. 4, it was possible to estimate the Donnan-equilibrium potential (approximately -7 mV) from the difference in reversal potential of current–voltage curves obtained in the same cell approximately 15 min apart; this correction has been applied to values of V_m in Fig. 4. The current–voltage relation is approximately linear over the range -110 to $+20$ mV and has a reversal potential of about $+3$ mV. Linear current–voltage relations with a reversal potential near 0 mV have also been obtained by voltage-clamp recordings with two conventional micro-electrodes from bull-frog hair cells (Corey & Hudspeth, 1979) and with gigohm-seal electrodes from solitary chick hair cells (Ohmori, 1985).

Adaptation. One feature of our recordings was the absence of adaptation in receptor currents during protracted stimulation. Adaptation was not observed in response to sinusoidal stimulation at frequencies ranging from 20 to 40 Hz (Fig. 3). Had such adaptation been present, it would have produced an asymmetry between the responses to alternate half-cycles of the stimulus. Adaptation was also not observed

in response to step stimulation (Fig. 10*A*), even for step durations exceeding 400 ms, during which it would have been expected to produce a gradual decay of the initial response amplitude. Finally, adaptation did not occur at the onset of the response to gated sinusoidal stimulation (Fig. 4*A*).

Mean–variance plots and the two-conductance-state model. We found no evidence of the discrete opening of single transduction channels in our experiments; for this reason, we could not directly measure the conductance of a single channel or the

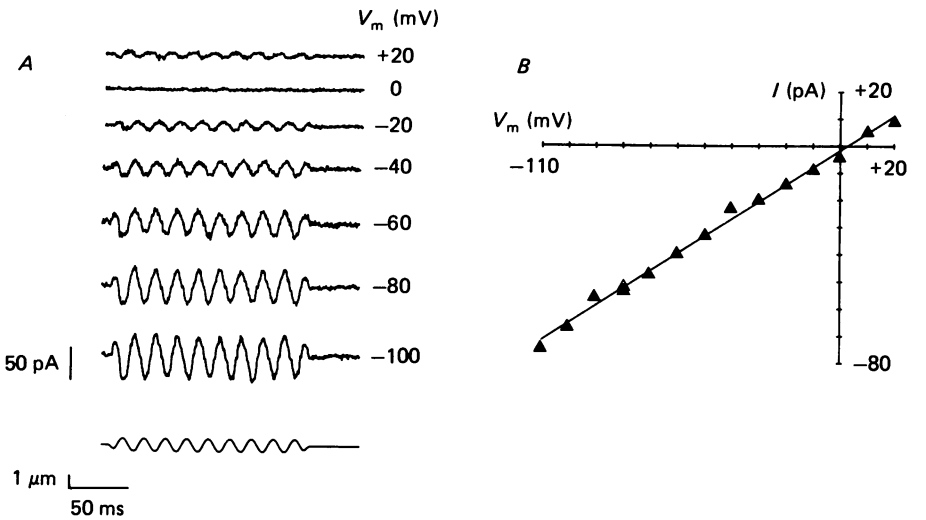

Fig. 4. Current–voltage relation. *A*, receptor-current wave forms measured at different values of membrane potential, V_m, in response to stimulation of the hair bundle by a gated sinusoid of 0·5 μm peak amplitude (lowest trace). The stimulus frequency was about 39 Hz and the stimulus duration was 256 ms. Wave forms have been digitally smoothed. V_m has been corrected for a Donnan-equilibrium potential of about −7 mV, a value measured in this cell from the difference in reversal potential of current–voltage curves acquired 15 min apart. *B*, current–voltage curve for the same cell. V_m was increased from −110 to +20 mV in 10 mV steps, followed by a return to −80 mV. At each value of V_m, the receptor current was measured in response to a gated sinusoid and the amplitude of the steady-state portion of the response was computed from the average of several response cycles. The continuous line, fitted to the data by minimum mean square error criteria, indicates a reversal potential of +3 mV.

number of transduction channels in a hair cell. We did observe, however, that receptor currents were noisy. Accordingly, we used the technique of ensemble-variance analysis to estimate the number of transduction channels and the single-channel conductance on the assumption that the transduction channel is governed by a two-conductance-state model. The two-conductance-state model of the transduction channel is derived in detail in the Appendix. The basic notion of this model is that the measured receptor current, I, is the sum of the currents through a large number, N, of identical, statistically independent channels, each of which can be in either a conducting (open) state with probability p, or a non-conducting (closed) state with probability $1-p$. When a channel is open, the single-channel current, i, flows. The model predicts that the mean and variance of the receptor current are related by a

parabolic function (eqn. (9)). In this section, we test this prediction and estimate values of N and i.

Fig. 5 illustrates the calculation of the mean, $\bar{I}$, and variance, σ^2, of the receptor current. Individual cycles of the response to sinusoidal hair-bundle displacement (Fig. 5*A*) were averaged to obtain the mean receptor current, $\bar{I}$ (Fig. 5*B*). The magnitude of $\bar{I}$ is maximum for large, positive hair-bundle displacements and approaches zero for large, negative displacements. The difference between each cycle

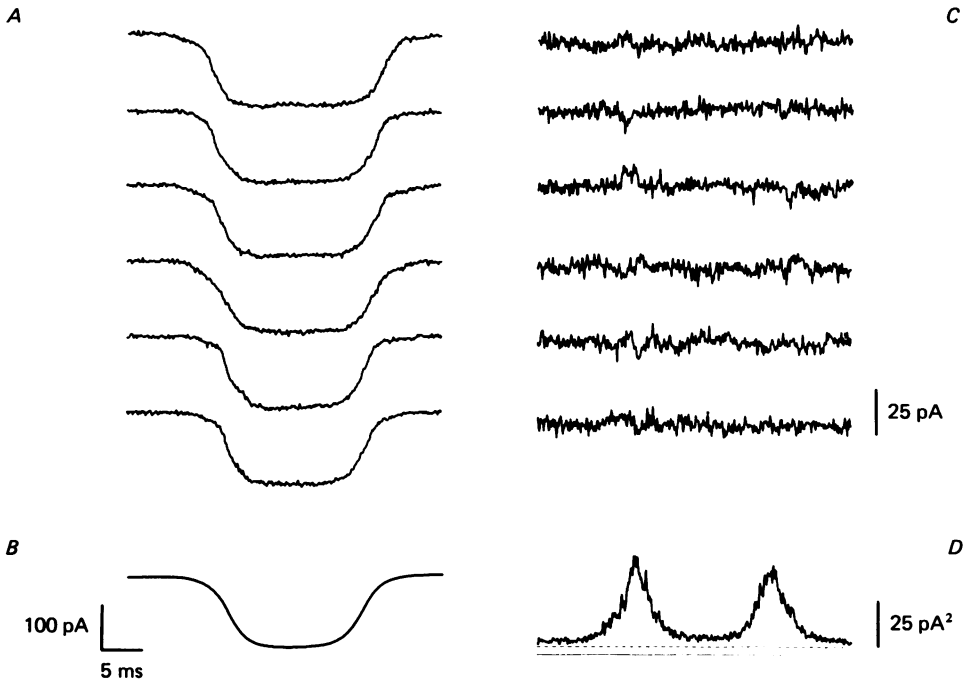

Fig. 5. Computation of the mean receptor current, $\bar{I}$, and variance, σ^2. *A*, individual cycles of the receptor current in response to a sinusoidal stimulus. *B*, the mean receptor current, $\bar{I}$, formed by averaging 136 cycles of the response. The response approaches zero for negative displacements and attains the maximum inward current value for positive displacements. *C*, the difference between the single receptor-current traces from *A* and the mean current $\bar{I}$, plotted on a magnified amplitude scale. The fluctuations of the receptor current about the mean are greatest at those times when the mean current is midway between positive and negative saturation. *D*, σ^2, the average variance of receptor current, computed by squaring and averaging the traces of *C*. σ^2 has two peaks, corresponding to the times when the mean current is not in saturation. A continuous line is drawn at $\sigma^2 = 0$. The dashed line is drawn at $\sigma_0^2 = 6$ pA², the lower bound suggested by an analysis of the sources of noise in whole-cell recording, as described in the text.

of the receptor current and the mean current appears greatest at times when the response is between its maximum and minimum saturated values (Fig. 5*C*). The average fluctuation of the individual cycles about the mean is measured by the receptor-current variance, σ^2, which is defined as the sum of the mean square differences between individual traces and the mean (Fig. 5*D*). The variance trace has two peaks at times corresponding to the rising and falling phases of $\bar{I}$.

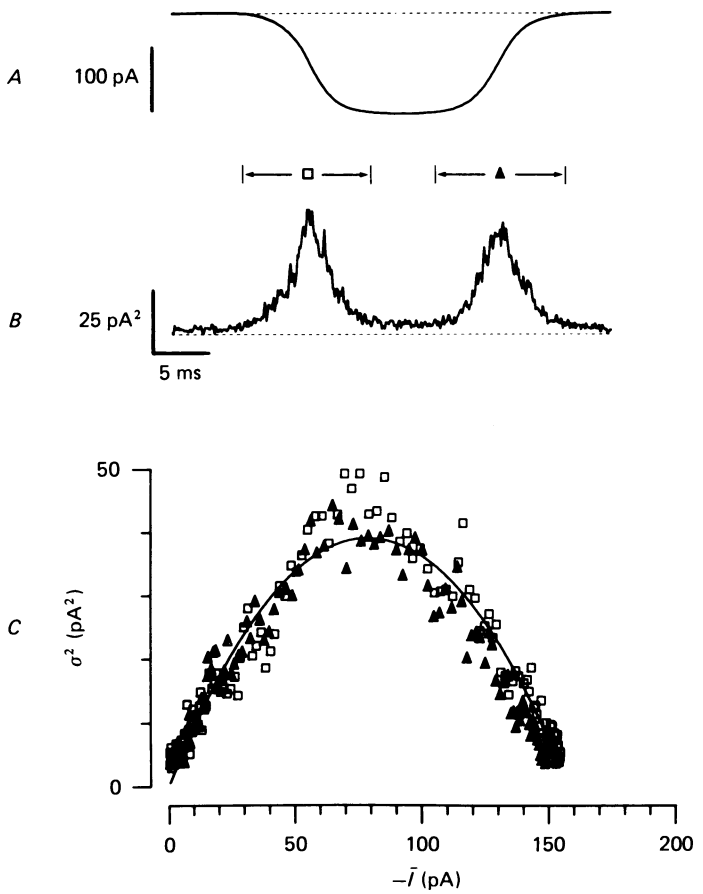

Fig. 6. Mean–variance plots for two half-cycles of the response. *A*, the mean receptor current, $\bar{I}$. The dashed line is the zero-current value, $\bar{I}_0$. *B*, the receptor-current variance, σ^2. The dashed line is the zero-variance level, σ_0^2. *C*, the mean–variance plot produced by plotting the instantaneous values of $\sigma^2(t)$ against $\bar{I}(t)$. Consistent with the previous literature of ensemble-variance analysis, we have plotted increasing magnitude of inward current along the positive abscissa. The open symbols are produced by plotting σ^2 against $\bar{I}$ for the falling phase of the receptor current (whose range is denoted by □ in *A* and *B*); the filled symbols are for the rising phase of the receptor current (whose range is denoted by ▲ in *A* and *B*). In accordance with the predictions of the two-conductance-state model, a parabola (eqn. (9)) has been fitted to the data from the superimposed plots by minimum mean square error criteria. From this parabola, values of the number of channels, N, and the single-channel current, i, can be estimated. For this cell, $N = 160$ and $i = -1{\cdot}00$ pA.

The relation between $\bar{I}$ and σ^2 is demonstrated in the mean–variance plot of Fig. 6*C*, in which the instantaneous value of $\sigma^2(t)$ is plotted against the instantaneous value of $I(t)$. The relation between σ^2 and $\bar{I}$ is a double-valued function: the same value of σ^2 occurs twice for each complete cycle of $\bar{I}$, once during the falling phase of $\bar{I}$ evoked by positive-going displacement, and once during the rising phase due to negative-going displacement. It is therefore possible to produce a mean–variance plot from each of the two half-cycles of the averaged response. These two sets of data are

superimposed in Fig. 6*C* (open and filled symbols) demonstrating that, within the temporal resolution of these measurements, the relation between σ^2 and $\bar{I}$ in this cell is instantaneous and without memory. In subsequent Figures we consider only data from those eighteen cells in which estimates of N and i obtained by fitting each half-cycle of the mean–variance plot separately were within 12% of the values obtained by fitting data from both half-cycles taken together.

The two-conductance-state model predicts that the relation between σ^2 and $\bar{I}$ is a parabolic function (eqn. (9)): σ^2 approaches zero as $\bar{I}$ approaches either zero or its maximum (inward) value, $\bar{I}_{max}$. In addition, σ^2 is maximum for $\bar{I} = \bar{I}_{max}/2$. This makes some intuitive sense, since by the model one would expect the variance in the receptor current to approach zero when all the transduction channels in a cell are either open ($\bar{I} = \bar{I}_{max}$) or closed ($\bar{I} = 0$). These predictions are borne out in the data. Fitting a parabola to the data in Fig. 6*C* according to eqn. (9) gives estimates of the values for two model parameters, the single-channel current, i, and the number of transduction channels per cell, N. For these data, $N = 160$ and $i = -1{\cdot}00$ pA. The values of N and i obtained by fitting separately the data for either half-cycle of the response (open or filled symbols) are within 5% of these numbers. The single-channel conductance, γ, computed from the data of Fig. 6*C* on the assumption that the channel has a reversal potential of 0 mV (eqn. (10)), is 11·8 pS.

For the two-conductance-state model, the maximum probability that a transduction channel is open, p_{max}, is equivalent to the peak fraction of channels open for a maximum positive hair-bundle displacement. p_{max} can be determined from eqn. (7) given estimated values of N and i, since $\bar{I}_{max} = Nip_{max}$. The value of p_{max} measured from the data in Fig. 6 is 1·00. The average value of p_{max} for all cells in which mean–variance plots were obtained is $0{\cdot}99 \pm 0{\cdot}08$ (mean ± S.D., $n = 18$). This means that essentially all the transduction channels in a hair cell are simultaneously opened by the largest positive mechanical stimulus.

Fig. 7 shows mean–variance plots for four cells, with maximum mean receptor-current amplitudes ranging from −28 to −160 pA. Data from each cell have been fitted with eqn. (9), from which values of N and γ have been estimated. These results illustrate two generally valid points. First, the single-channel conductance does not vary systematically with the maximum receptor-current size. The average value of γ in these four cells is $12{\cdot}4 \pm 0{\cdot}7$ pS (mean ± S.D.) at 10 °C. Secondly, the value of N is proportional to response size, as expected from eqn. (7). Cells with smaller response amplitudes do not have smaller single-channel conductances, but only fewer active transduction channels. The relation between the maximum response size and number of transduction channels for all eighteen cells is shown in Fig. 8*A*. In order to compare data from cells held at different membrane potentials, V_m, the maximum receptor-current amplitude of each cell has been normalized by V_m to obtain the maximum conductance, G_{max}. The data support the prediction of the two-conductance-state model, derived from eqn. (7), that G_{max} is proportional to N: $G_{max} = N\gamma p_{max}$. Fig. 8*B* shows that the value of γ is not correlated with G_{max}. The average value of γ for the eighteen cells studied in detail is $12{\cdot}7 \pm 2{\cdot}7$ pS (mean ± S.D.). Fig. 8 includes data for one cell in which G_{max} decreased by a factor of two over the course of several minutes of recording. In this cell, the estimated value of N also decreased by about

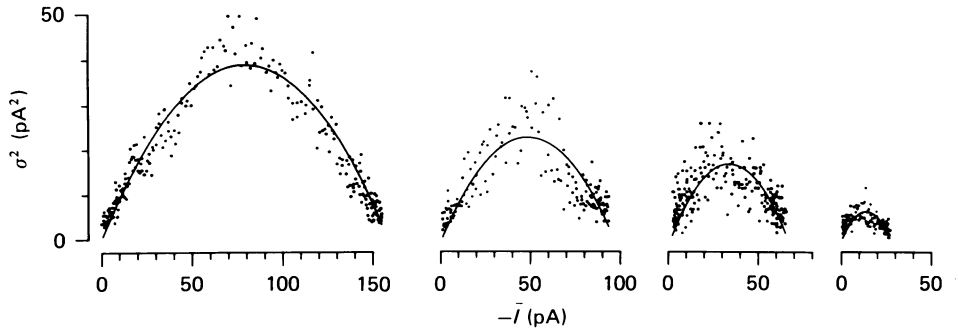

Fig. 7. Mean–variance plots for four cells with different maximum response amplitudes. The leftmost data, replotted from Fig. 6*C*, are from a cell with a maximum receptor current of −160 pA. The other three traces, plotted on the same scale, are from cells with maximum responses of −102, −73 and −28 pA. Each plot has been fitted with eqn. (9) from which values of N and γ have been estimated. For these cells, the values of N are 160, 106, 68 and 30; the values of γ are 11·8, 12·3, 13·4 and 12·1 pS. This suggests that N varies in proportion to response size, whereas γ does not vary systematically.

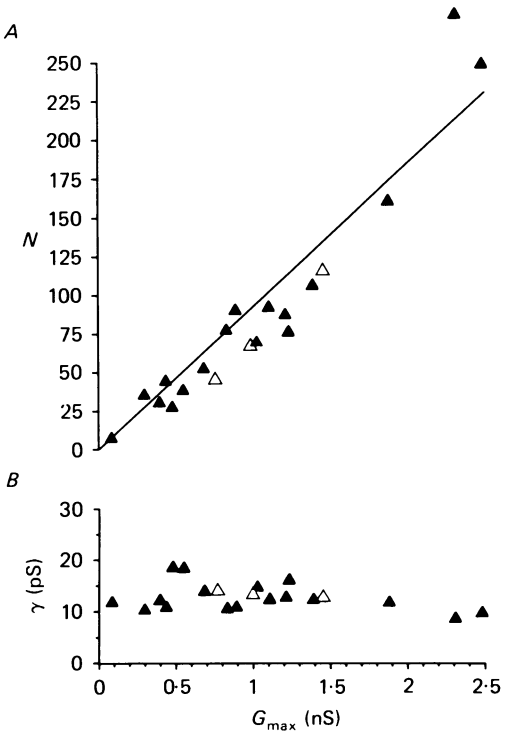

Fig. 8. The relation N and γ to G_{max}, the maximum transduction conductance of a cell. *A*, values of N and *B*, values of γ estimated from mean–variance plots for eighteen cells, plotted against the maximum conductances of the cells, G_{max}. These data show that N is proportional to G_{max} while γ does not appear to vary systematically. The open symbols show values of N and γ estimated in one cell at different times as its response decreased. The straight line in the upper panel is a regression line fitted according to $G_{max} = N\gamma p_{max}$ with $p_{max} = 0{\cdot}99$.

a factor of two while the estimate of γ varied by only about 10 %. This finding suggests that the receptor current declines as the number of transduction channels decreases, possibly as the channels become mechanically disrupted by over-stimulation.

False-variance artifacts. We have assumed that the receptor-current variance we measure arises solely from stochastic properties of the transduction channel as expressed by the two-conductance-state model. This assumption underlies the estimation of N and i by fitting mean–variance plots with eqn. (9). There are, however, several possible artifacts in these experiments that could generate a 'false' receptor-current variance, whose dependence on mean current resembles that expected from the model, but which does not reflect the stochastic properties of the channel. In this section we consider the two most important false variance artifacts.

Potentially the most serious false variance artifact can occur if noise in the motion of the stimulus probe is transduced by the hair cell into variance in the receptor current. Probe-motion noise could result if sound or vibration, generated by the equipment or in the building, were coupled to the probe through the air or through an imperfect vibration-isolation table. It could also result from electrical noise in the driving circuitry for the probe stimulator, from thermal motion of the probe and from convective currents in the solution in the experimental chamber. This small probe noise would be added to the large, intentionally applied sinusoidal motion of the probe. Fig. 9 shows a simulation of this false-variance artifact. In the simulation we have assumed that the relation between hair-bundle displacement and receptor current is instantaneous and non-stochastic so that *all* the variance in the receptor current results from transduction of probe noise. At any position of the hair bundle, x, the r.m.s. amplitude of the receptor-current noise, $\sigma_n(x)$, will be proportional to the slope of the displacement–response curve, $d\bar{I}(x)/dx$, which is a function of x. Thus, the receptor-current variance, $\sigma_n^2(x)$, is given by

$$\sigma_n^2(x) = (\sigma_p \, d\bar{I}(x)/dx)^2, \tag{5}$$

where σ_p is the r.m.s. noise of the probe's motion. For large positive or negative hair-bundle displacements, $\bar{I}(x)$ is in saturation either at its maximum value or at zero. At these extremes of displacement, $d\bar{I}(x)/dx$ approaches zero, so $\sigma_n^2(x)$ also approaches zero. However, for hair-bundle displacements between these two extremes, probe-motion noise is transduced into receptor-current noise that reaches a maximum where $d\bar{I}(x)/dx$ is maximum. Plotting $\sigma_n^2(x)$ against $\bar{I}(x)$ produces a false mean–variance plot. The shape of this false mean–variance plot resembles to some extent the real mean–variance plot expected from inherent properties of the transduction channel. If the magnitude of the false variance were substantial, estimates of the number of transduction channels and the single-channel current obtained by mean–variance plots would be incorrect.

To determine the extent to which probe-motion noise is a source of the receptor-current variance we used a photodiode as described in the Methods section and found σ_p, the noise of probe motion in the absence of intentional stimulation, to be at most 2 nm (r.m.s.). Then we computed $(d\bar{I}(x)/dx)^2$ from displacement–response curves for representative cells, used eqn. (5) to estimate σ_n^2, and compared this false variance with σ^2, the receptor-current variance actually measured in the same cells. Fig. 9*A* shows the displacement–response curve for the cell whose mean variance plot is shown in Fig. 6*C*. The maximum sensitivity of this cell is approximately 500 pA/μm. Given

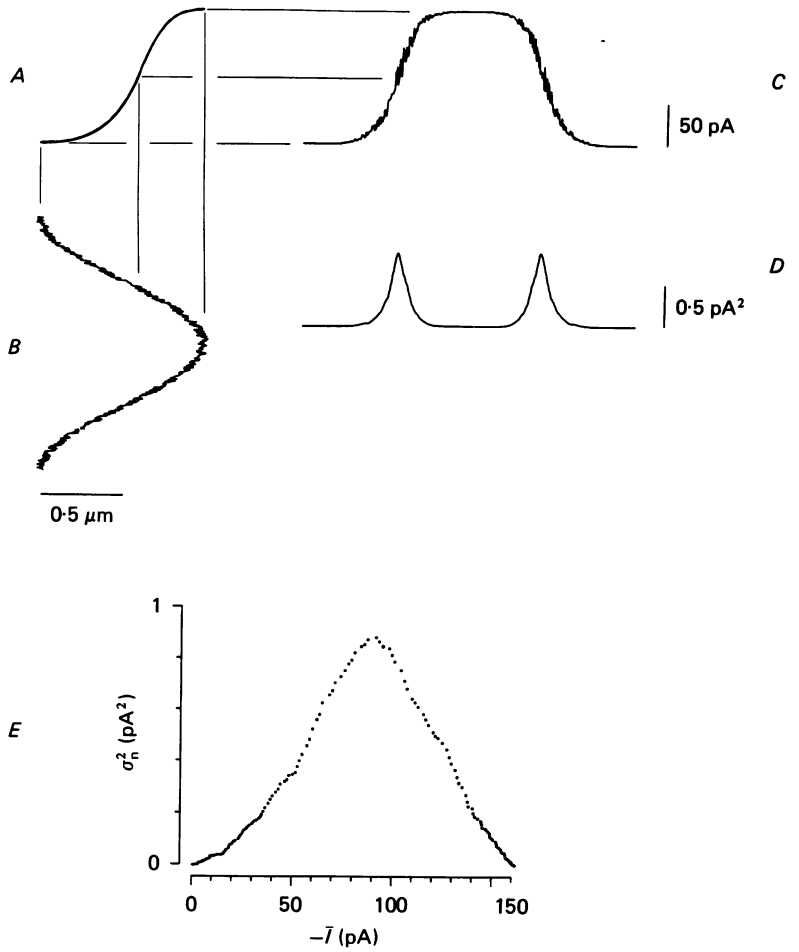

Fig. 9. Simulation of the false-variance artifact caused by transduction of noise in the motion of the stimulus probe. *A*, a displacement–response curve, a plot of receptor-current magnitude against probe position, taken from the cell whose mean–variance plot is shown in Fig. 6. *B*, the wave form of probe motion simulated by adding random noise with a nominal r.m.s. amplitude of 2 nm to a sinusoidal stimulus motion with a nominal peak amplitude of 0·5 μm. *C*, the wave form of receptor current anticipated from the transduction of the stimulus in *B* by a cell whose displacement–response relation is shown in *A*. *D*, the variance of the simulated receptor-current wave form, σ_n^2, due entirely to transduced probe-motion noise. σ_n^2 approaches zero as $\bar{I}$ approaches zero or $\bar{I}_{max}$ and is greatest where the slope of the displacement–response curve is maximum. *E*, a false mean–variance plot, which is a plot of σ_n^2 against the mean receptor current, $\bar{I}$, on the assumption that the r.m.s. amplitude of the probe motion is 2 nm. In order to make them clearly visible, the probe noise in *B* and the receptor-current noise in *C* have been exaggerated 10-fold.

an r.m.s. probe noise of 2 nm, the expected false variance, $\sigma_p^2(d\bar{I}(x)/dx)^2$, will have a peak amplitude of 0·9 pA² (Fig. 9*D*). A false mean–variance plot (Fig. 9*E*) can be generated by plotting the false variance against the mean current, $\bar{I}(x)$. Comparing this false mean–variance plot with the real mean–variance plot for this cell (Fig. 6*C*) shows that the maximum variance expected from transduced probe noise is over

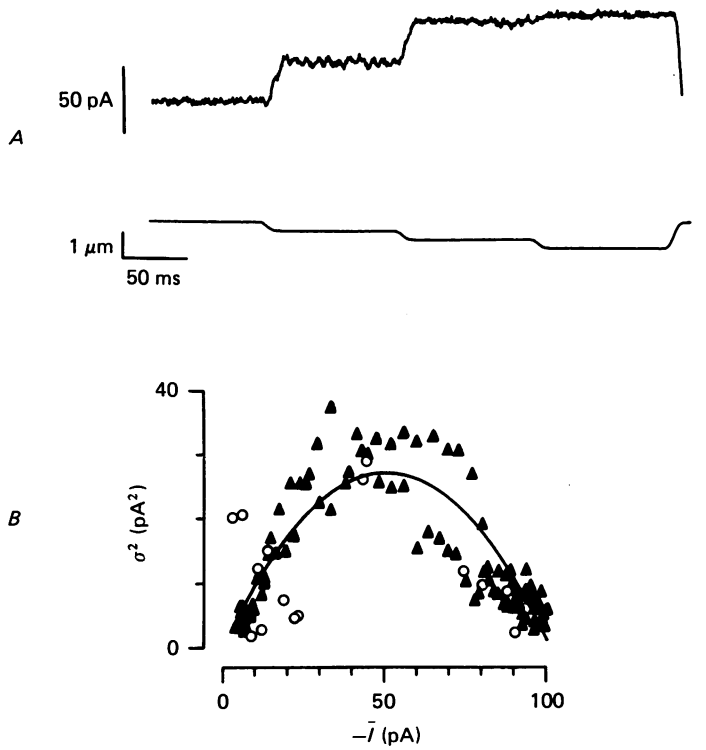

Fig. 10. A test for false variance due to slipping of the stimulus probe. *A*, the receptor-current wave form (upper panel) evoked by stimulation of the hair bundle with a staircase displacement of three equal steps, alternately negative-going (lower panel) and positive-going (not shown). *B*, mean–variance plots constructed from this cell's response to two stimulus paradigms: sinusoidal stimuli (▲) and step stimuli (○). The mean–variance plot for step stimuli was obtained by calculating the mean and variance of the steady-state portion (the last 70 %) of the receptor current evoked by each step. The parabola is fitted by eqn. (9) to the data for sinusoidal stimuli.

50-fold lower than the maximum receptor-current variance actually measured. Moreover, the false mean–variance curve of Fig. 9*E* is bell shaped whereas the real mean–variance plot of Fig. 6*C* is parabolic. These results indicate that transduction of probe noise is not the mechanism responsible for the experimentally observed variance in the receptor current. The same conclusion can be reached by determining what amplitude of probe-motion noise would have to exist if all the measured receptor-current variance were due to transduced probe noise. Given a peak receptor-current variance of 50 pA^2 and a maximum hair-cell displacement sensitivity of 500 pA/μm, eqn. (5) suggests that σ_p would have to be 14 nm. This amplitude of motion is almost an order of magnitude above our measurement noise floor; we would have been able to detect such a noise of probe motion had it been present.

A second artifact of probe motion that would produce a false receptor-current variance can occur if the probe slips with respect to the hair bundle, so that the receptor current evoked by an individual cycle or group of cycles differs substantially from the average current derived by summing the responses to a number of cycles. The response of the aberrant cycles would then contribute disproportionately to the

variance, distort the mean–variance plots, and lead to incorrect estimation of N and i. To test for this artifact, we measured $\bar{I}$ and σ^2 during the steady-state portion of the response to a staircase displacement of the hair bundle (Fig. 10*A*). In the steady state, neither the bundle nor the probe is moving, so the receptor-current variance we measure should be due solely to intrinsic properties of the channel. Although this step-stimulus paradigm yields fewer points than the sinusoidal-stimulus paradigm, the relations between $\bar{I}$ and σ^2 derived from these two paradigms overlap (Fig. 10*B*). For this reason, we believe it is unlikely that variations in probe coupling contribute substantially to the variance in receptor current we have measured in response to the sinusoidal-stimulus paradigm.

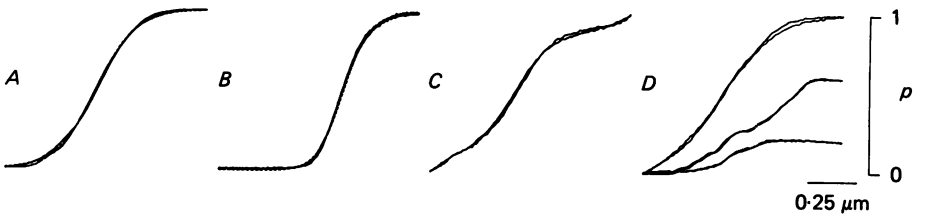

Fig. 11. Normalized displacement–response curves for four cells. Normalized displacement–response curves provide an estimate of $p(x)$ as described in the text. The superimposition of the rising and falling phases of the receptor current in response to a sinusoidal stimulus reflects the close coupling between the hair bundle and the probe. These examples show the variability in the shape of $p(x)$ encountered in this study. *A*, symmetrical. This curve has been fitted with a two-kinetic-state model (eqn. (16)), with $Z = 5{\cdot}8$ kcal/mol μm. $\bar{I}_{max} = -151$ pA. *B*, asymmetrical. This curve has been fitted with a three-kinetic-state model (eqn. (27)), with $Z_1 = 6{\cdot}7$ and $Z_2 = 3{\cdot}8$ kcal/mol μm. $\bar{I}_{max} = -128$ pA. *C*, irregular. $\bar{I}_{max} = -48$ pA. *D*, unstable. The three displacement–response curves were obtained from one cell several minutes apart. The data are plotted on a common scale, normalized to the initial response amplitude of -114 pA.

Gating of the transduction channel

Because we cannot detect the openings of single transduction channels, we cannot measure directly the kinetic properties of single channels. However, we can infer important gating properties from our receptor-current data. In the next section, we estimate the equilibrium probability that the channel is open as a function of displacement, $p(x)$, from displacement–response curves; we find that $p(x)$ is consistent with the predictions of a simple 'two-kinetic-state' model of the transduction channel. On the assumption of this model, we estimate the mean open lifetime of the channel from the power-spectral density of the receptor-current noise.

Displacement–response curves. Displacement–response curves were produced by plotting the instantaneous magnitude of the receptor current against the position of the hair bundle. Fig. 11 shows the range of shapes of displacement–response curves recorded from thirty cells in fourteen experiments. In this and subsequent Figures, both half-cycles of the response have been superimposed to demonstrate that hysteresis is negligible. In most (twenty-two) cells, the displacement–response curves were symmetrical and saturating, as in Fig. 11*A*. More asymmetrical, saturating

curves were recorded in three cells, as shown in Fig. 11*B*, and there were four cells in which the displacement–response curves were neither symmetrical nor saturating, as shown in Fig. 11*C*. In a few cells, the shape of the displacement–response curve changed with time; the shape of the curve was initially symmetric, but became increasingly irregular as the response size diminished (Fig. 11*D*). This effect may be a consequence of long, high-amplitude stimulation, during which the connexions of

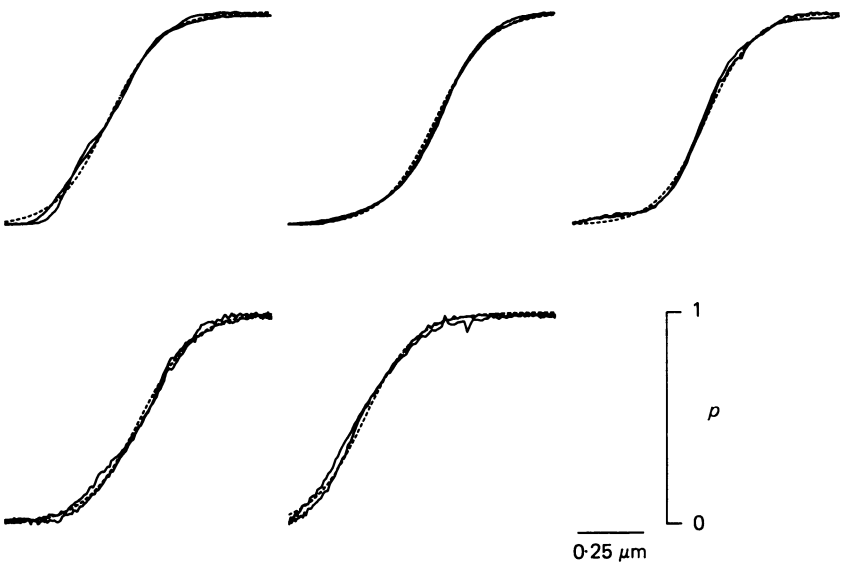

Fig. 12. Symmetrical displacement–response curves from cells with different response amplitudes. Examples of symmetrical normalized displacement–response curves are shown for five cells with maximum response amplitudes (reading from top left to bottom right) of −202, −160, −85, −54 and −28 pA. These curves have been fitted with the two-kinetic-state model (eqn. (16)). The values of Z for the cells are 5·9, 5·6, 6·2, 5·4 and 5·7 kcal/mol μm.

stereocilia to each other or to the kinocilium (for review, see Hudspeth, 1983) become more compliant. If this were to happen, the stereocilia would not move synchronously and the transduction channels would not be simultaneously activated with the result that the displacement–response curve is irregular. In the following sections we concentrate on the symmetrical, saturating displacement–response curves which were measured in the majority of cells.

Fig. 12 shows normalized displacement–response curves from five cells with response amplitudes ranging from −28 to −202 pA. By the two-conductance-state model, $\bar{I}(x)$ is directly proportional to $p(x)$, the probability that a given single channel is open (eqn. (7)). Therefore, normalizing the displacement–response curve by $\bar{I}_{max} = Nip_{max} \sim Ni$ gives an estimate of $p(x)$. The shapes of the normalized displacement–response curves in Fig. 12 are independent of the maximum response amplitude. This result is consistent with a premise of the two-conductance-state model, namely that $p(x)$ is not itself a function of N or i.

The two-kinetic-state model. The symmetrical, saturating and sigmoidal form of $p(x)$ in Fig. 12 suggests that a simple kinetic model might be sufficient to describe the behaviour of the transduction channel. One such model, termed the two-kinetic-state model, is described in detail in the Appendix. This model treats the transduction channel as having only two kinetically distinguishable states, one open and one closed, with the energy barrier between the open and closed states modelled as being linearly proportional to the displacement of the hair bundle (Corey & Hudspeth, 1983*b*). For this model, $p(x)$ is given by eqn. (16). Fitting eqn. (16) to the data of Fig. 12 allows us to estimate Z, the displacement sensitivity of the free-energy change between the open and closed states. The value of Z for the curves in Fig. 12 is $5{\cdot}7 \pm 0{\cdot}3$ kcal/mol μm (mean $\pm$ S.D., $n = 5$). Fits of eqn. (16) to the displacement–response curves from cells with response amplitudes ranging from -20 to -202 pA yielded values of Z ranging from 4·4 to 8·4 kcal/mol μm ($5{\cdot}7 \pm 1{\cdot}1$ kcal/mol μm, or $39{\cdot}7 \pm 7{\cdot}7$ fN/molecule, mean $\pm$ S.D., $n = 18$). The value of Z did not correlate with response amplitude, again suggesting that $p(x)$ is not a function of N or i. The range of Z values we measured is comparable to that obtained by fitting the two-kinetic-state model to transepithelial-current data (Corey & Hudspeth, 1983*b*).

Most of the displacement–response curves in these experiments, such as those shown in Fig. 12, were adequately fitted by the two-kinetic-state model. In order to assess the sufficiency of this model, we also attempted to fit the predictions of a three-kinetic-state model to these data. This model, which is detailed in the Appendix, consists of one open state and two closed states; access to each of the closed states is assumed to be dependent on the position of the hair bundle. The equilibrium probability of the channel's being open is then described by an equation with four free parameters (eqn. (27)), including two displacement sensitivities of free-energy change, Z_1 and Z_2. This model has been shown to fit displacement–response curves of transepithelial current (Corey & Hudspeth, 1983*a*). A measure of the symmetry of the displacement–response curves is the ratio Z_2/Z_1. In curves that are completely symmetrical, Z_2/Z_1 is zero and the three-kinetic-state model becomes equivalent to a two-kinetic-state model (eqn. (16)) with $Z_1 = Z$. As displacement–response curves become increasingly asymmetrical Z_2/Z_1 increases. The curve in Fig. 11*A* is the most symmetrical seen in these experiments: $Z_2/Z_1 = 4 \times 10^{-3}$. The curve in Fig. 11*B* is one of the most asymmetrical: $Z_2/Z_1 = 0{\cdot}6$. In only three cells was Z_2/Z_1 greater than 0·6. In these cells, the three-state model with its additional two free parameters fit the data somewhat better than did the two-state model. But in most cells, Z_2/Z_1 was below 0·2 (for example, for the data in Fig. 12, $Z_2/Z_1 = 0{\cdot}2 \pm 0{\cdot}1$ (mean $\pm$ S.D., $n = 5$)). For these cells we concluded that the two-kinetic-state model was sufficient to fit the displacement–response curves. In a few cells (e.g. Fig. 11*C*) neither the two- nor the three-state model fit the data adequately.

In a previous section, we found that the relation between the mean receptor current $\bar{I}$, and the receptor-current variance, σ^2, is predicted by the two-conductance-state model of the transduction channel (eqn. (9)). The two-kinetic-state model makes a further prediction about the relation between $\bar{I}$ and σ^2. As derived in the Appendix (eqn. (19)), the two-kinetic-state model predicts that σ^2 is directly proportional to the derivative of mean current with respect to displacement, $\mathrm{d}\bar{I}/\mathrm{d}x$, with a constant of proportionality equal to Z/iRT, where R and T have their usual thermodynamic

meanings. Fig. 13 shows a test of this prediction for two cells; values of Z/i of $-6{\cdot}3$ and $-6{\cdot}4$ kcal/mol μm pA were obtained by fitting straight lines to the data of Fig. 13*C*. For each cell, Z/i can also be computed by dividing the value of Z obtained from the displacement–response curve by the value of i obtained from the mean–variance plot. For the data shown in Fig. 13, the estimates of Z/i obtained in this way are $-5{\cdot}7$ and $-5{\cdot}6$ kcal/mol μm pA. Although the analysis of the data in Fig. 13 does not produce independent estimates of the values of either Z or i, it does serve to check the consistency of the two-kinetic-state model with the data

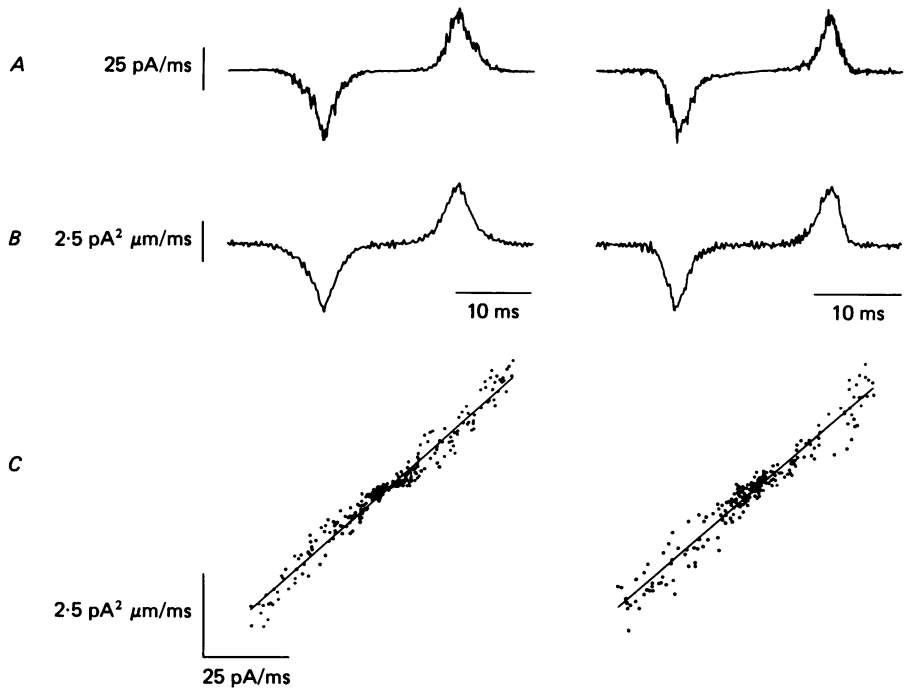

Fig. 13. Plot of $d\bar{I}/dt$ against σ^2 for two cells. *A*, $d\bar{I}/dt$, the derivative of the mean receptor current. The derivative has been digitally smoothed. The data in the left panels are from the cell whose mean–variance plot is shown in Fig. 6*C*. *B*, $-A\omega \sin(\omega t+\phi)\,\sigma^2(t)$, which by the two-kinetic-state model (eqn. (20)) is proportional to $d\bar{I}/dt$. *C*, a plot of $d\bar{I}/dt$ (from *A*) against $-A\omega \sin(\omega t+\phi)\,\sigma^2(t)$ (from *B*); the data fall on a straight line with slope $-Z/iRT$. The values of Z/i measured from the slope of the regression lines fitted to these data by minimum mean square error criteria are $-6{\cdot}3$ and $-6{\cdot}4$ kcal/mol μm pA.

Power-spectral density. Power-spectral densities of receptor-current noise were obtained in only three cells from records of the receptor current evoked in response to displacement steps, as in Fig. 10*A*. These data were not adequate to attempt accurate fits of different kinetic models of the transduction channel, but they were sufficient to suggest a value of the mean open time of the channel on the assumption that the two-kinetic-state model is valid. The data in Fig. 2*B* derive from a cell in which $Z_2/Z_1 = 0{\cdot}2$, indicating that the displacement–response data from this cell were adequately fit by this model. The corner frequency of the spectrum in Fig. 2*B*, f^*, is approximately 250 Hz. These data were obtained in response to a step displacement

that elicited a mean current of approximately 0·3 $\bar{I}_{max}$, corresponding to an open-channel probability, $p = 0{\cdot}3$. Given these values for f^* and p, eqn. (23) can be used to estimate a mean open time, $t_o = 0{\cdot}9$ ms at 9·5 °C. If the rate constants governing the two-state model have a Q_{10} of approximately 2·1 (Corey & Hudspeth, 1983*b*), the estimated mean open time of the transduction channel for $p = 0{\cdot}3$ would be 130 μs at 37 °C. At lower values of p (i.e. more negative hair-bundle displacements), the mean open time of the channel would be expected to decrease.

DISCUSSION

The conductance of the transduction channel

In this study, we have employed the whole-cell, gigohm-seal voltage-clamp technique to record receptor currents from individual hair cells and have used ensemble-variance techniques to infer properties of the transduction channel. The data obtained are consistent with a two-conductance-state model of the transduction channel; the average single-channel conductance is 12·7 pS at 10 °C. As expected from the model, there appears to be no systematic relation between the single-channel conductance and the cell's maximum conductance. The transepithelial receptor current of hair cells is known to be carried well by the alkali cations, but less well by other ions of slightly larger hydrated radius. These results and the permeability-ratio measurements made with the gigohm-seal technique (Ohmori, 1985) suggest that the transduction channel is a hydrated pore with a diameter near 0·7 nm (Corey & Hudspeth, 1979). Assuming, then, that the channel is an aqueous pore whose conductivity increases with increasing temperature with a Q_{10} of about 1·3 (Hille, 1984, p.49), the transduction-channel conductance should be about 17 pS at room temperature (22 °C), and about 25 pS at 37 °C. This value of conductance is similar to that of another poorly selective channel, the acetylcholine receptor, which has a range of 20–40 pS (for review, see Hille, 1984, p.222).

In the inner ear, the transduction current is probably carried primarily by K^+ (Corey & Hudspeth, 1979; Crawford & Fettiplace, 1979; Russell, 1983). In our recordings, with Na^+ the predominant cation in the extracellular fluid, the transduction current was carried largely by Na^+. To assess accurately the channel's conductance in its normal ionic environment, it is necessary to correct for the difference in the channel's permeabilities to the two ions. Transduction-current measurements in the bull-frog's sacculus (Corey & Hudspeth, 1979) and reversal-potential determinations in the chick's vestibular system (Ohmori, 1985) show that Na^+ and K^+ carry transduction current equally well to within 10 %. The conductance of transduction channels *in situ* is therefore likely to be near that estimated in this study. In our recordings, the cytoplasmic cations were largely replaced by Cs^+. Since Cs^+ carries transduction current efficiently (Corey & Hudspeth, 1979; Ohmori, 1985), it is unlikely to have blocked the influx of Na^+ significantly.

The number of transduction channels

The number of transduction channels per hair cell, N, ranges from several dozen to several hundred and is proportional to G_{max}. It is not clear whether this variability in N and G_{max} represents the inherent variation among normal cells or, more likely

in our view, differing degrees of damage to cells which natively would have had uniformly large responses. It is clear, however, that the largest transduction currents observed in this study are comparable with those found in voltage-clamp recordings with two conventional micro-electrodes (Corey & Hudspeth, 1979) and would produce receptor potentials in the range of amplitudes encountered in single-electrode recordings (Hudspeth & Corey, 1977). Accordingly, we believe that data from cells with the largest responses provide a reasonable estimate of the number of transduction channels natively present in saccular hair cells of the bull-frog. We note that there may be additional channels in the cells, chemically similar to the transduction channel, which are not activatable by mechanical stimuli.

It has been suggested (Hudspeth, 1982; Pickles, Comis & Osborne, 1984) that the transduction channels are located at or near the tips of the stereocilia. Our estimate of the maximum number of transduction channels is intriguing because, were the channels equally distributed among the stereocilia, this number would correspond to only a few, perhaps four, channels per stereocilium. Morphological approaches such as freeze-fracture electron microscopy might well be able to demonstrate membrane specializations corresponding to this small number of transduction channels.

The band width of the variance measurements in these experiments generally extended from a low frequency of 20–40 Hz (imposed by the duration of the average of σ^2) to a high frequency of 5 kHz (imposed by the sampling interval). Had we been able to extend the low-frequency limit of the measurement to 0 Hz, we would expect, on the assumption of the two-kinetic-state model, that the measured values of σ^2 would have been 5–10% higher. Estimates of i obtained by fitting eqn. (9) to mean–variance plots would also have been higher by this amount, and estimates of N commensurately lower. Most of the spectral energy in the receptor current occurs below 1 kHz (Fig. 2) while most of the spectral energy of the background noise occurs above 1 kHz. Thus, although we usually used a high-frequency band width limit of 5 kHz, it would have been possible to have chosen a limit nearer 1 kHz in order to increase the signal-to-noise ratio of our recordings. Reducing the band width would not have changed any of our conclusions, though it probably would have further reduced our estimate of the upper bound on $p_{\min}$ (eqn. 4).

Gating of the transduction channel

The results of this study are consistent with a model of the transduction channel (Appendix) in which the gating of the channel is directly controlled by a mechanical linkage with the hair bundle. Such a linkage, for example a bridge between adjacent stereocilia (Pickles *et al.* 1984), might be particularly vulnerable to mechanical trauma, such as that resulting from over-stimulation of hair bundles. Our findings that the maximum transduction conductance of a cell correlates with the number of transduction channels (Fig. 8*A*), both in a population of cells and within an individual cell, suggests that the response decreases as transduction channels or their mechanical linkages become disrupted due to over-stimulation. This disruption may be the molecular correlate of the acoustic trauma that follows exposure to loud sounds.

The minimum probability that a transduction channel is open, $p_{\min}$, is approximately zero and the maximum probability that the channel is open, $p_{\max}$, is approximately one. These results suggest that saturating, physiological stimuli can

completely modulate the channel's open probability: large negative displacements simultaneously close all channels, and large positive displacements simultaneously open them. In this sense, the transduction process is highly efficient. As detailed in the Appendix, the observation that $p_{max} = 1$ also implies that the displacement-controlled step of the transduction process is between the open state of the transduction channel and the immediately adjacent closed state (C_1 and O in eqn. (24)). The response latency of a channel operating according to such a model can be shorter than that of a channel described by a model in which the displacement-sensitive step occurs between two closed states. Our results do not, however, rule out the possibility that other open or closed states exist, with displacement-independent rate constants governing their transitions.

The power spectra of the receptor current show that the gating of the transduction channel is rapid. These data are consistent with those from the transepithelial current in the saccular macula evoked by *en masse* step displacements of the hair bundles of many cells, which show an increase within 15 μs of stimulation and can reach a steady state in less than 100 μs (Corey & Hudspeth, 1983*b*). This fast gating of the transduction channel seems necessary to explain the ability of some hair cells to transduce mechanical stimuli at frequencies exceeding 100 kHz.

The transduction channel in the hair cell appears to be different from the stretch-sensitive ion channel found in a tissue-cultured preparation of embryonic chick skeletal muscle (Guharay & Sachs, 1984). In contrast with our results from hair cells, analysis of single-channel data in the muscle preparation is consistent with a kinetic model having one open state and three closed states, with the mechanically sensitive transition between two of the closed states (C_3 and C_2 in our notation).

Displacement–response curves

Most displacement–response curves recorded in this study were symmetrical, as in Fig. 12. A kinetic model of the transduction channel comprising one open state and one closed state appears sufficient to fit these displacement–response curves. However, as mentioned above, the data do not rule out the possibility that other, displacement-independent, open or closed states exist, with transitions between these states governed by displacement-independent rate constants. The effect of the additional states on the displacement–response curve would depend on the values of these rate constants. If the rate constants were fast compared with the frequency of hair-bundle stimulation, the effect of the additional states would be to change the value of G in eqn. (16), which is equivalent to shifting the curve along the x axis. These other states would not affect the shape of the curve, which is determined by Z. If, on the other hand, the rate constants were slow, one would expect different relaxation times for channel opening and channel closing. This effect would produce displacement–response curves whose rising phase has a steeper or shallower slope than the falling phase. It is difficult to determine from our data (Figs. 11 and 12) whether or not this effect occurs.

In a few cells the displacement–response curves were asymmetrical. For these cells, a model having two displacement-controlled transitions, between C_1 and O and between C_2 and C_1, fits the displacement–response curves somewhat better than did the simple two-kinetic-state model. It is possible that these few cells were the only

ones in which some or all of a natively present asymmetry in the transduction process was preserved. However, the results for these cells are well within a large range of shapes of displacement–response curves, from highly symmetrical to highly irregular, seen among cells or within a single cell as a function of time (Fig. 11). We therefore do not wish to exaggerate the importance of the curves that were somewhat better fitted by a three-state model.

In contrast to the generally symmetrical displacement–response curves obtained in this study, displacement–response curves derived from receptor potentials (Hudspeth & Corey, 1977; Crawford & Fettiplace, 1981) and from transepithelial currents (Corey & Hudspeth, 1983*a*) are markedly asymmetrical. It is difficult to compare directly the data from the present study of individual voltage-clamped cells with the transepithelial-current data representing the summed currents of a number of cells of somewhat different orientation. Furthermore, there are no compelling data from two-electrode voltage-clamp studies of hair cells that demonstrate an asymmetry in displacement–response curves. Hence, we are unable to resolve the possible discrepancy between the present data and those of other studies. However, in the discussion that follows, we will *assume* that the displacement–response curves of hair cells are natively asymmetrical, and suggest ways in which the process of making whole-cell recordings could alter the transduction process, making these curves more symmetrical. Even if this assumption were correct, the two-conductance-state model would still apply to the data, and the estimates of the number of transduction channels in a cell and of the single-channel conductance would be unchanged.

If displacement–response curves become symmetrical as a consequence of gigohm-seal recording, they must do so either upon contact of the electrode with the cell, or within a minute after the rupture of the membrane patch, which is the time it takes us to compensate for the electrode's series resistance, attach the stimulus probe and start recording from the cell. The response could become symmetrical immediately as a result of a mechanical distortion of the cuticular plate, or upon formation of the gigohm seal. Such a distortion might also occur as a consequence of rupturing the membrane under the recording electrode. Alternatively, the response might change as a result of the rapid replacement of the cytoplasmic fluid of the cell by the internal solution in the electrode after the membrane is ruptured. Based on the rate at which Cs^+ blocks the cell's K^+ channels, equilibration of the cell's interior for small ions is appreciable within a minute after establishing fluid contact with the cell. The internal solution contains low, buffered concentrations of free Ca^{2+} and H^+, whereas the normal concentrations of these ions in the cell are unknown. Thus, it is possible that a change in the concentration of Ca^{2+} or H^+ in the neighbourhood of the transduction channels alters their properties. The diffusion of large cytoplasmic factors from the cell is a slower process (Fenwick *et al.* 1982) and is therefore less likely to play a role in altering the displacement–response curves.

There are several ways one can imagine that mechanical or chemical effects might make displacement–response curves symmetrical. One view is that the transduction channel is natively described by a kinetic model with several displacement-controlled transitions between states. The process of whole-cell recording might remove or alter access of the channel to some states, thereby making the channel act as if there were only a single displacement-sensitive transition. The data from transepithelial-current

recordings (Corey & Hudspeth, 1983*b*) suggest that the number of natively present displacement-controlled transitions would have to be large for such a model to explain the response kinetics. Accordingly, for this view to be correct, the process of making the whole-cell recordings must selectively make displacement independent all transitions between states except that between C_1 and O (eqn. (24)). Another, perhaps more economical, interpretation is the feed-back model of the transduction channel detailed in the Appendix (eqns. (28) and (29)). By this model, the transduction channel natively has only one displacement-dependent transition, between C_1 and O, and one displacement-independent transition, between C_2 and C_1; we allow the rate constant (k_{21}) governing the transition between C_2 and C_1 to depend on the concentration of a rapidly diffusible messenger substance, S (which could, for example, be Ca^{2+} or H^+). For this model, the steady-state flow of S into the cell through the transduction channels is proportional to the receptor current, which is a function of $p(x)$; increasing the concentration of S in turn increases the value $p(x)$. This means that there is a positive feed-back between the concentration of S and the amplitude of the receptor current. Such a process can produce highly asymmetrical displacement–response curves when the feed-back loop is intact, and symmetrical curves when the loop is broken. Thus, if the process of recording from cells acts to cut the feed-back loop, for example by keeping the concentration of S constant (i.e. by buffering the internal concentration of Ca^{2+} or H^+), the displacement–response curves will be made more symmetrical.

Adaptation

In this study, the receptor current showed negligible adaptation to continuous or intermittent sinusoidal stimuli or to step stimuli, even for durations exceeding 400 ms. By contrast, transepithelial currents (Eatock, Corey & Hudspeth, 1979; Corey & Hudspeth, 1983*a*), receptor potentials and receptor currents of single cells (Eatock & Hudspeth, 1981) all show marked adaptation to sinusoidal and step stimuli with durations under 100 ms. The source of this discrepancy is unknown. It is possible that the lack of adaptation in the whole-cell recordings is due to the loss of cytoplasmic constituents or to the buffering of the H^+ and Ca^{2+} concentrations in the internal solution. There is evidence (Eatock *et al.* 1979) that the effect of adaptation is to shift the displacement–response curve along the abscissa. In terms of the two-kinetic-state model, this is equivalent to changing G (eqn. (16)), and thus can be viewed as a change in $p(x)$. Adaptation need not act by producing an inactivation of channels (a change in N) or a change in conductance, γ.

Discrete openings of single transduction channels?

We have not observed discrete, single-channel events in our recordings. Moreover, we would not expect to resolve such single-channel openings under our experimental conditions: the single-channel currents are small, the number of channels in a cell is large and their mean open time is brief. These conclusions differ from those reached in studies of whole-cell recordings from solitary hair cells of the chick (Ohmori, 1984, 1985), in which step discontinuities in the receptor current were evoked by low-frequency stimulation of the hair bundle. These steps in current were interpreted as resulting from the opening of individual transduction channels. If this interpretation

is correct, chick hair cells have only about ten activatable transduction channels; the conductance of each channel is about 50 pS at 28–32 °C. In addition, records of the receptor current evoked by step stimuli (e.g. Fig. 11 of Ohmori, 1985) suggest that the mean open time of the transduction channel in chick hair cells exceeds 100 ms at 37 °C.

An alternative explanation of these data is that the step discontinuities in receptor current represent, not openings and closings of individual transduction channels, but the conjoint gating of larger numbers of transduction channels. This interpretation is suggested by two observations. First, step discontinuities in the current do not appear to occur at random times, as would be expected for a channel with stochastically distributed openings; rather, they occur at nearly the same points in each cycle of the response (e.g. Figs. 2, 4 and 8 in Ohmori, 1985). This suggests that a repeatable artifact of the hair bundle's motion is being transduced into discontinuities in the receptor current. Secondly, the current steps evoked by hair-bundle deflexion are not uniformly square in shape as would be expected for single-channel openings, nor do they approach the steady state exponentially, as might be expected if the receptor current were filtered by the characteristics of the recording system. The current steps instead show an unusual overshoot suggesting either that the transduction channels in chick hair cells have multiple subconductance states, or that the recorded currents result from transduced artifacts of hair-bundle motion. We believe it is possible that the stimulus paradigm used in the experiments, which involves grazing the tips of the stereocilia with the stimulus probe, sequentially activates either individudal stereocilia, or ranks of stereocilia of similar length. As more stereocilia are recruited, the receptor current would increase proportionally (Hudspeth & Jacobs, 1979). Thus, the steps in the current recordings may actually represent the activation of several transduction channels of smaller conductance and shorter mean open time than reported.

APPENDIX

Models of the hair-cell transduction channel

In this section, we analyse two models of the transduction channel and detail the properties of these models that bear on our experimental results. The 'two-conductance-state model' is a general formulation which makes predictions about the number of transduction channels in the cell and their single-channel conductance. The 'two-kinetic-state model' is a specific example of a two-conductance-state model which makes predictions about the form of the displacement–response curve and the kinetic properties of the transduction channel. In addition, we briefly consider some properties of channel models having more than two kinetic states.

The two-conductance-state model. The chief assumption of this model is that the receptor current, I, measured in a hair cell in response to displacement of the hair bundle, is the sum of the individual currents, q_j, of N identical, statistically independent, transduction channels:

$$I = \sum_{j=1}^{N} q_j. \tag{6}$$

At any instant, a given transduction channel exists in either one of two conductance states: a conducting state with probability p, or a non-conducting state with probability $1-p$. In the conducting state, the current through the single channel, q_j, equals the single-channel current, i; in the non-conducting state, $q_j = 0$. The two-conductance-state model does not specify how many *kinetically* distinguishable open and closed states a channel has, only that all open states have the same conductance, and that all closed states have zero conductance. The probability that the channel is open, p, is an instantaneous function of hair-bundle displacement, x, but a precise specification of $p(x)$ is not necessary for this analysis.

By taking the mean and variance of eqn. (6) it is easily shown that

$$\bar{I} = Nip, \tag{7}$$

$$\sigma^2 = Ni^2p(1-p), \tag{8}$$

where $\bar{I}$ is the mean receptor current and σ^2 is the variance of the current. Eqns. (7) and (8) can be combined to eliminate the explicit dependence on p:

$$\sigma^2 = \bar{I}i - \bar{I}^2/N. \tag{9}$$

Eqn. (9) predicts that a plot of σ^2 against $\bar{I}$, which we term the mean–variance plot, follows a parabola. By fitting a parabola to the mean–variance plot, values of N and i can be estimated. On the assumption that the channel is ohmic, the single-channel conductance can be estimated by dividing the estimated single-channel current by the driving force on the ions that carry the transduction current:

$$\gamma = i/(V_m - V_{rev}), \tag{10}$$

where V_m is the membrane potential and V_{rev} is the reversal potential for ions flowing through the channel, which we take to be zero (Fig. 4).

The two-kinetic-state model. The observation that the displacement–response curves measured in this study are generally symmetrical, saturating and sigmoidal suggests a particularly simple kinetic model of the transduction channel (Corey & Hudspeth, 1983*b*). This model is a specific case of the two-conductance-state model that has only two kinetically distinguishable states, one closed state, C_1, and one open state, O:

$$C_1 \underset{k_{01}}{\overset{k_{10}}{\rightleftharpoons}} O, \tag{11}$$

where k_{10} and k_{01} are, respectively, the opening and closing rate constants of the process. To allow us to extend our descriptions of kinetic-state models to include those with a number of closed states (see below), our nomenclature for the state names (i.e. C_1 and O) and for the rate constants (i.e. k_{01} and k_{10}) differs from that of Corey & Hudspeth (1983*b*). The rate constants are assumed to depend on the energy required for the transduction channel to make a transition between the open and closed states:

$$k_{10} = (kT/h)\, e^{-(G_I + \delta\Delta G)/RT}, \tag{12}$$

$$k_{01} = (kT/h)\, e^{-(G_I - (1-\delta)\Delta G)RT}, \tag{13}$$

where G_I is the height of the intrinsic energy barrier of the transition, ΔG is the energy

difference between open and closed states and δ ($0 \leqslant \delta \leqslant 1$) is the fraction of ΔG that contributes to the energy barrier between C_1 and O; h, k, R and T have their usual thermodynamic meanings. The energy difference, ΔG, is assumed to be linearly related to hair-bundle displacement, x:

$$\Delta G = G - Zx, \tag{14}$$

where G is a displacement-independent term and Zx is a displacement-sensitive term, with Z being the displacement sensitivity. For the two-kinetic-state model, the equilibrium probability that the channel is in the open state, p, is given by (Colquhoun & Hawkes, 1977):

$$p = \left(1 + \frac{k_{01}}{k_{10}}\right)^{-1}. \tag{15}$$

Substituting eqns. (12) and (13) into eqn. (15) gives:

$$p(x) = (1 + e^{\Delta G/RT})^{-1} = (1 + e^{(G-Zx)/RT})^{-1}. \tag{16}$$

Eqn. (16) is the explicit functional relation between p and x predicted by the two-kinetic-state model. $p(x)$ has a symmetrical, sigmoidal shape, with $p_{\min} = p(-\infty) = 0$ and $p_{\max} = p(+\infty) = 1$.

Eqns. (16) and (7) predict the shape of the displacement–response curve. From eqn. (7), the displacement–response curve, $\bar{I}(x)$, is proportional to $p(x)$. When $\bar{I}(x)$ is normalized by dividing it by its maximum value, $\bar{I}_{\max} = Nip_{\max} = Ni$, the resulting normalized displacement–response curve is $p(x)$; by fitting eqn. (16) to this curve, we can estimate the values of G and Z.

The relation between the mean and variance of the receptor current for the two-conductance-state model (eqn. (9)) was derived without specifying $p(x)$. Eqn. (16) gives $p(x)$ for the two-kinetic-state model and thus imposes a further constraint on the relation between σ^2 and $\bar{I}$. Differentiating eqn. (7) gives

$$\frac{d\bar{I}}{dx} = Ni\frac{dp}{dx}. \tag{17}$$

dp/dx is obtained by differentiating eqn. (16):

$$\frac{dp}{dx} = \frac{Z}{RT}p(1-p). \tag{18}$$

Combining eqns. (17), (18) and (8) yields

$$\frac{d\bar{I}}{dx} = \frac{Z}{RT}Nip(1-p) = \frac{Z/i}{RT}\sigma^2. \tag{19}$$

This equation states that, for a transduction channel described by the two-kinetic-state model, the derivative of the receptor current with respect to displacement is directly proportional to the receptor-current variance. By fitting a line to a plot of σ^2 against $d\bar{I}/dx$, the ratio Z/i can be estimated. In our experiments the hair bundle was displaced as a sinusoidal function of time (Fig. 3), $x(t) = -A\cos(2\pi ft + \phi)$, where f is the stimulus frequency and ϕ is the phase of the probe's motion with respect to

the driving signal, and A is the peak amplitude of the probe's motion. Hence, eqn. (19) can be written

$$\frac{\mathrm{d}\bar{I}}{\mathrm{d}t} = \frac{Z/i}{RT}\sigma^2 A 2\pi f \sin(\omega t + \phi). \tag{20}$$

The two-kinetic-state model also makes predictions about the mean length of time the channel spends in the open state, the mean open time. The power-spectral density of the receptor-current noise, $S_I(f)$, for the two-kinetic-state model (Colquhoun & Hawkes, 1977) is

$$S_I(f) = \frac{2\sigma^2}{\pi f^*}\frac{1}{1+(f/f^*)^2}, \tag{21}$$

where f^* is the corner frequency of the spectrum,

$$f^* = \frac{k_{01}+k_{10}}{2\pi} = \frac{k_{01}}{2\pi(1-p)}. \tag{22}$$

$S_I(f)$ depends on hair-bundle position because both σ^2 and f^* are functions of x. The mean open time of the channel, t_o, is equal to ${k_{01}}^{-1}$. From eqn. (22),

$$t_o = {k_{01}}^{-1} = (2\pi(1-p)f^*)^{-1}. \tag{23}$$

The analysis leading to the derivation of eqns. (16) and (19) is based on the assumption that the channel is in equilibrium at each value of x. This assumption is valid as long as x changes slowly compared to the equilibrium time constant for the system. This time constant, $(k_{01}+k_{10})^{-1} = (2\pi f^*)^{-1}$, is the rate at which p approaches its equilibrium value (given by eqns. (15) and (16)) following a perturbation. In these experiments f^* exceeds 200 Hz and the frequency of stimulation is at most 40 Hz. It is therefore reasonable to conclude that the channel's open probability is effectively in equilibrium throughout a displacement of the hair bundle.

Models with more than two kinetic states. The two-kinetic-state model of eqn. (11) can be extended to include more than one closed state:

$$\ldots \mathrm{C}_2 \underset{k_{12}}{\overset{k_{21}}{\rightleftharpoons}} \mathrm{C}_1 \underset{k_{01}}{\overset{k_{10}}{\rightleftharpoons}} \mathrm{O}, \tag{24}$$

For such models, the equilibrium probability of the channel being open is

$$p = \left(1+\frac{k_{01}}{k_{10}}\left(1+\frac{k_{12}}{k_{21}}(1+\ldots)\right)\right)^{-1}. \tag{25}$$

If only *one* pair of rate constants in eqn. (25) is dependent on displacement (e.g. k_{01} and k_{10}, or k_{12} and k_{21}) in the manner described by eqns. (12) and (13), then eqn. (25) can be reduced to the form

$$p(x) = p_{\max}(1+\mathrm{e}^{(G'-Zx)/RT})^{-1}, \tag{26}$$

where Z is identical to the value in eqn. (16) and G' differs from G in eqn. (16) by an amount that depends on ratios of the rate constants for displacement-independent transitions between closed states. If the first pair of rate constants (i.e. k_{01} and k_{10})

is the only displacement-dependent pair of terms, $p_{max} = 1$ and the effect of displacement-independent transitions between closed states on $p(x)$ is to change the value of G in eqn. (16), which is equivalent to shifting the displacement–response curve along the x axis. If k_{12} and k_{21} are the only displacement-dependent terms, the displacement–response curve will be shifted along the abscissa and in addition $p_{max} < 1$. The observation in our receptor-current data that p_{max} is approximately one suggests that the transition between C_1 and O is the displacement-sensitive one.

If *two* pairs of rate constants, k_{10}/k_{01} and k_{21}/k_{12}, are displacement-sensitive, eqn. (25) can be written as

$$p(x) = (1+e^{\Delta G_1/RT}(1+e^{\Delta G_2/RT}))^{-1}, \tag{27}$$

where $\Delta G_1 = G_1 - Z_1 x$ and $\Delta G_2 = G_2 - Z_2 x$. Normalized displacement–response curves that are fitted by eqn. (27) can be asymmetrical. For large positive displacements (at which $\exp(\Delta G_2/RT) \ll 1$). Eqn. (27) asymptotically approaches eqn. (16) with $\Delta G = \Delta G_1$. For large negative displacements, eqn. (27) approaches eqn. (16) with $\Delta G = \Delta G_1 + \Delta G_2$. For this model, the degree of symmetry of the displacement–response curves can be summarized by the ratio Z_2/Z_1.

Finally, we briefly consider a feed-back model of the transduction channel. This model has three states, C_2, C_1 and O, as in eqn. (24). The rate constants for the transition between C_1 and O are displacement sensitive, as given by eqns. (12) and (13). The rate constants for transitions between C_2 and C_1 are not explicitly displacement sensitive; however, the forward rate constant, k_{21}, is made a function of the intracellular concentration of a substance, S, that diffuses through the open transduction channel or whose concentration is otherwise altered by channel opening. If changes in the intracellular concentration of S are rapid compared to the time course of hair-bundle stimulation, the concentration of S will be directly proportional to p. We can then write k_{12}/k_{21} in the form

$$\frac{k_{12}}{k_{21}} = (a_0 + a_1 p^m)^{-1}, \tag{28}$$

where a_0 and a_1 are constants and we permit the possibility that k_{21} depends on the simultaneous binding of m molecules of S. Substituting eqns. (12), (13) and (28) into eqn. (25) gives

$$p^{m+1} - \alpha p^m + p(a_0 - \alpha + 1)/a_1 - \alpha a_0/a_1 = 0, \tag{29}$$

where $\alpha = (1+\exp(\Delta G/RT)^{-1}$. Solving eqn. (29) for each position of the hair bundle gives $p(x)$, the normalized displacement–response curve. This is a feed-back model because the concentration of S is a function of p, while the value of p depends on the concentration of S. This model produces displacement–response curves whose symmetry depends on the strength of the feed-back, as determined by the constants a_0 and a_1. For a given value of a_1, the displacement–response curve is symmetrical for large values of a_0 and becomes increasingly asymmetrical as a_0 decreases.

We thank Richard Jacobs for technical assistance and production of the Figures, Richard Lewis for helpful discussions during the experiments, Jonathon Howard for discussions leading to our estimate of p_{min} and Steven Lisberger for the use of the oscillator. We thank Jonathon Howard, Richard Lewis, Villu Maricq, Aline McKenzie and Luis Robles for their comments on the manuscript. Preliminary experiments in this project were supported by National Institutes of Health grants NS20429, NS13154 and NS07024; principal support was provided by the System Development Foundation and by National Institutes of Health grants NS22389 and NS22536.

REFERENCES

COLQUHOUN, D. & HAWKES, A. G. (1977). Relaxation and fluctuations of membrane currents that flow through drug-operated channels. *Proceedings of the Royal Society* B **199**, 231–262.

COREY, D. P. & HUDSPETH, A. J. (1979). Ionic basis of the receptor potential in a vertebrate hair cell. *Nature* **281**, 675–677.

COREY, D. P. & HUDSPETH, A. J. (1980). Mechanical stimulation and micromanipulation with piezoelectric bimorph elements. *Journal of Neuroscience Methods* **3**, 183–202.

COREY, D. P. & HUDSPETH, A. J. (1983*a*). Analysis of the microphonic potential of the bullfrog's sacculus. *Journal of Neuroscience* **3**, 942–961.

COREY, D. P. & HUDSPETH, A. J. (1983*b*). Kinetics of the receptor current in bullfrog saccular hair cells. *Journal of Neuroscience* **3**, 962–976.

CRAWFORD, A. C. & FETTIPLACE, R. (1979). Reversal of hair cell responses by current. *Journal of Physiology* **295**, 66*P*.

CRAWFORD, A. C. & FETTIPLACE, R. (1981). Non-linearities in the responses of turtle hair cells. *Journal of Physiology* **315**, 317–338.

EATOCK, R. A., COREY, D. P. & HUDSPETH, A. J. (1979). Adaptation in a vertebrate hair cell: stimulus-induced shift of the operating range. *Society for Neuroscience Abstracts* **5**, 19.

EATOCK, R. A. & HUDSPETH, A. J. (1981). Adaptation in hair cells: *in vitro* intracellular responses and *in vivo* microphonic potentials from a vestibular organ. *Society for Neuroscience Abstracts* **7**, 62.

FENWICK, E. M., MARTY, A. & NEHER, E. (1982). A patch-clamp study of bovine chromaffin cells and of their sensitivity to acetylcholine. *Journal of Physiology* **331**, 577–597.

GUHARAY, F. & SACHS, F. (1984). Stretch-activated single ion channel currents in tissue-cultured embryonic chick skeletal muscle. *Journal of Physiology* **352**, 685–701.

HAMILL, O. P., MARTY, A., NEHER, E., SAKMANN, B. & SIGWORTH, F. J. (1981). Improved patch-clamp techniques for high-resolution current recording from cells and cell-free membrane patches. *Pflügers Archiv* **391**, 85–100.

HILLE, B. (1984). *Ionic Channels of Excitable Membranes*. Sunderland: Sinauer.

HOLTON, T. & HUDSPETH, A. J. (1984). Transduction current in saccular hair cells examined with the whole-cell voltage-clamp technique. *Society for Neuroscience Abstracts* **10**, 10.

HOLTON, T. & HUDSPETH, A. J. (1985). A study of the hair-cell transduction channel using the whole-cell voltage-clamp technique. *Abstracts of the Eighth Midwinter Research Meeting of the Association for Research in Otolaryngology* **8**, 48–49.

HUDSPETH, A. J. (1982). Extracellular current flow and the site of transduction by vertebrate hair cells. *Journal of Neuroscience* **2**, 1–10.

HUDSPETH, A. J. (1983). Mechanoelectrical transduction by hair cells in the acousticolateralis sensory system. *Annual Review of Neuroscience* **6**, 187–215.

HUDSPETH, A. J. & COREY, D. P. (1977). Sensitivity, polarity, and conductance change in the response of vertebrate hair cells to controlled mechanical stimuli. *Proceedings of the National Academy of Sciences of the U.S.A.* **74**, 2407–2411.

HUDSPETH, A. J. & JACOBS, R. (1979). Stereocilia mediate transduction in vertebrate hair cells. *Proceedings of the National Academy of Sciences of the U.S.A.* **76**, 1506–1509.

HUDSPETH, A. J. & KROESE, A. B. A. (1983). Voltage-dependent interaction of dihydrostreptomycin with the transduction channels in bullfrog sensory hair cells. *Journal of Physiology* **345**, 66*P*.

LEWIS, R. S. & HUDSPETH, A. J. (1983). Voltage- and ion-dependent conductances in solitary vertebrate hair cells. *Nature* **304**, 538–541.

MARTY, A. & NEHER, E. (1983). Tight-seal whole-cell recording. In *Single-Channel Recording*, ed. SAKMANN, B. & NEHER, E., pp. 107–122. New York: Plenum.

NEHER, E. & STEVENS, C. F. (1977). Conductance fluctuations and ionic pores in membranes. *Annual Review of Biophysics and Bioengineering* **6**, 345–381.

OHMORI, H. (1984). Mechanoelectrical transducer has discrete conductances in the chick vestibular hair cell. *Proceedings of the National Academy of Sciences of the U.S.A.* **81**, 1888–1891.

OHMORI, H. (1985). Mechano-electrical transduction currents in isolated vestibular hair cells of the chick. *Journal of Physiology* **359**, 189–217.

PICKLES, J. O., COMIS, S. D. & OSBORNE, M. P. (1984). Cross-links between stereocilia in the guinea pig organ of Corti, and their possible relation to sensory transduction. *Hearing Research* **15**, 103–112.

RUSSELL, I. J. (1983). Origin of the receptor potential in inner hair cells of the mammalian cochlea – evidence for Davis' theory. *Nature* **301**, 334–336.

SEILER, N. & SCHMIDT-GLENEWINKEL, T. (1975). Regional distribution of putrescine, spermidine and spermine in relation to the distribution of RNA and DNA in the rat nervous system. *Journal of Neurochemistry* **24**, 791–795.

SHOTWELL, S. L., JACOBS, R. & HUDSPETH, A. J. (1981). Directional sensitivity of individual vertebrate hair cells to controlled deflection of their hair bundles. *Annals of the New York Academy of Sciences* **374**, 1–10.

SIGWORTH, F. J. (1980). The variance of sodium current fluctuations at the node of Ranvier. *Journal of Physiology* **307**, 97–129.

SIGWORTH, F. J. (1983). Electronic design of the patch clamp. In *Single-Channel Recording*, ed. SAKMANN, B. & NEHER, E., pp. 3–35. New York: Plenum.

WERSÄLL, J., BJORKROTH, B., FLOCK, Å. & LUNDQUIST, P.-G. (1973). Experiments on ototoxic effects of antibiotics. *Advances in Oto-Rhino-Laryngology* **20**, 14–41.